HHS Public Access

Author manuscript

Mol Psychiatry. Author manuscript; available in PMC 2022 September 17.

Published in final edited form as:

Mol Psychiatry. 2022 June ; 27(6): 2833–2848. doi:10.1038/s41380-022-01512-y.

Chronic stress disrupts the homeostasis and progeny progression of oligodendroglial lineage cells, associating immune oligodendrocytes with prefrontal cortex hypomyelination

Alexandros G. Kokkosis[1,2], **Miguel M. Madeira**[1], **Matthew R. Mullahy**[1], **Stella E. Tsirka**[1,*]

[1]Department of Pharmacological Sciences, Renaissance School of Medicine at Stony Brook University, Stony Brook, New York

[2]Current address: Neuroscience Functional Modeling Group - RGC Biology, Regeneron Pharmaceuticals, Tarrytown, NY 10591

Abstract

Major Depressive Disorder (MDD) is a chronic debilitating illness affecting yearly 300 million people worldwide. Oligodendrocyte-lineage cells have emerged as important neuromodulators in synaptic plasticity and crucial components of MDD pathophysiology. Using the repeated social defeat (RSDS) mouse model, we demonstrate that chronic psychosocial stress induces long-lasting losses and transient proliferation of oligodendrocyte-precursor cells (OPCs), aberrant differentiation into oligodendrocytes, and severe hypomyelination in the prefrontal cortex. Exposure to chronic stress results in OPC morphological impairments, excessive oxidative stress, and oligodendroglial apoptosis, implicating integrative-stress responses in depression. Analysis of single-nucleus transcriptomic data from MDD patients revealed oligodendroglial-lineage dysregulation and the presence of immune-oligodendrocytes (Im-OL), a novel population of cells with immune properties and myelination deficits. Im-OL were also identified in mice after RSDS, where oligodendrocyte-lineage cells expressed immune-related markers. Our findings demonstrate cellular and molecular changes in the oligodendroglial lineage in response to chronic stress and associate hypomyelination with Im-OL emergence during depression.

*Correspondence to: Dr. Stella E. Tsirka, Department of Pharmacological Sciences, Renaissance School of Medicine at Stony Brook University, Stony Brook, NY 11794-8651, Tel: 631-444-3859, Fax: 631-444-9749, styliani-anna.tsirka@stonybrook.edu.

Author Contributions

A.G.K. and S.E.T. conceptualized the project. A.G.K. designed, performed, and analyzed experiments. M.M.M. wrote the code and performed bioinformatic analyses, image quantification and data analyses. M.R.M. performed image quantification, Neurolucida tracing and data analyses. A.G.K., M.M.M, and S.E.T drafted and edited the manuscript. S.E.T. provided technical expertise, funding, and supervised the project.

Competing Interests statement

The authors declare no competing interests.

Introduction

Oligodendrocyte precursor cells (OPCs) are glia with heterogeneous homeostatic properties, ubiquitously present in the central nervous system (CNS)[1]. Although they are highly proliferative, optimal OPC density and distribution are under tight self-regulation[2,3]. They serve both as progenitors of myelinating oligodendrocytes (OLs), and as active surveyors of their local environment integrating neuronal activity by establishment of direct neuroglial contacts[4–6]. As the neuromodulatory roles of OPCs have started to emerge[1,7], the extent of their contribution to neuropsychiatric disorders and specifically major depressive disorder (MDD) has come into focus. Recent work revealed that OPC loss due to chronic psychosocial stress in the medial prefrontal cortex (mPFC) was sufficient to impede astrocytic activity, lead to neuronal dysfunction and depressive-like behavior[8]. A single-nucleus transcriptomics (sn-RNAseq) study from the PFC of MDD patients revealed that gene expression changes occurred predominantly in the OPCs and deep-layer excitatory neurons, further supporting that myelination and synaptic plasticity play a crucial role in the pathogenesis of depression[9]. Notably, oligodendrogenesis and myelination were reported to be highly sensitive to psychosocial input and stressful experiences[10,11]. Recent evidence has demonstrated significant myelin deficits in animal studies modeling depression[12–15]. Corresponding OL-related transcriptional deficits and white matter (WM) structural abnormalities have been implicated in the pathophysiology of MDD[16–18], further supporting a pathophenotypic connection between depression and oligodendroglial-lineage cells (OLN).

The mPFC is a highly evolved brain region affecting top-down executive functions (personality expression, decision-making, social behavior)[19] and processing of fear/aversive-related stimuli[20]. Prolonged psychosocial stress can exert detrimental effects on the frontal cortex, strongly associating mPFC to MDD pathophysiology[21]. Such effects include volume and connectivity reductions in emotional/cognitive circuitry, significant myelin deficits and destabilization/loss of synaptic connections[22]. Corresponding reductions were identified in glial populations in the mPFC from postmortem studies of MDD patients, and in animal models of depressive-like behavior[23]. Although oligodendroglial dysfunction is a hallmark of MDD pathophysiology, the cellular and molecular mechanisms of the OLN compromises remain unclear.

Here, we utilize a chronic psychosocial stress mouse model and a snRNA-seq dataset from MDD patients[9], to investigate: the extent to which chronic stress affects the OPC homeostasis and temporal dynamics of these perturbations; whether chronic stress has modulatory effects on OLN progression and OL maturation in MDD patients and the depression animal model; and what cellular and molecular mechanisms underlie these events.

Results

Chronic stress induces depressive-like behavior leading to OPC reductions and time-dependent alterations of their proliferation in the mPFC.

The repeated social defeat paradigm (RSDS; 10 days) was used to induce depressive-like behavior in adult male mice[8,24] (Fig. 1a). Twenty-four hours after RSDS (D10) behavioral tests were performed (BH; D11-D14) and the socially defeated (SD) mice were divided (see Methods) in two groups: SD-Sus (~80%; susceptible to stress) and SD-Res (~20%; resilient to stress). Both groups exhibited significant anxiety-like behavior, however the SD-Sus additionally demonstrated characteristic depressive-like phenotypic features: social avoidance, despair-like behavior, reduction of reward under stress and anhedonia (Fig. 1b–c, Supplementary Fig. 1a–d).

To determine the effects of chronic stress on OPC density and proliferation in the mPFC, 5-Bromo-2′-deoxyuridine (BrdU) was administered *ad libitum* throughout RSDS, and experimental groups were analyzed 15 days later. Histological analysis of the mPFC revealed a significant reduction of OPC density (platelet-derived growth factor receptor alpha; PDGFRα$^+$) and OPC proliferation (%Ki67$^+$ of PDGFRα$^+$) in SD-Sus compared to Con and SD-Res mice (Fig. 1d–f; Supplementary Fig. 2d). Additionally, a moderate decrease of BrdU$^+$ label-retaining OPCs (%BrdU$^+$ of PDGFRα$^+$) and a significant reduction of their proliferation capacity (%Ki67$^+$BrdU$^+$ of PDGFRα$^+$) were detected in SD-Sus compared to Con and SD-Res groups (Fig. 1g–h). Analogous reductions of OPC density and proliferation capacity in SD-Sus groups were confirmed with the OPC marker chondroitin sulfate proteoglycan 4 (CSPG4) and immunoblot analyses of PDGFRα and CSPG4 (Supplementary Fig.2a–c). These results indicate that chronic stress induces significant disturbances in OPC homeostasis.

The moderate decrease of BrdU$^+$ OPCs in the SD-Sus (%BrdU$^+$ of PDGFRα$^+$/CSPG4$^+$) (Fig. 1g, Supplementary Fig. 2f) in conjunction with the significant increase of total BrdU$^+$ cells in the mPFC on D15 (Supplementary Fig. 2e) prompted us to characterize the early effects of psychosocial stress on OPCs. Therefore, we utilized a short-term RSDS paradigm adaptation (miniSD; 3 days) followed by 3 days of behavioral tests (BH; D4-D6), which resulted in ~50% of the SD mice becoming SD-Sus (Supplementary Fig. 3a–f). Histological analysis of mPFC revealed a significant reduction of OPCs (evident by reduced EGFP+ cells from the PDGFRα$^+$ and *CSPG4*-EGFP$^+$ mouse lines) and OLN-cell marker oligodendrocyte transcription factor 2 (Olig2) in the SD-Sus (Supplementary Fig. 3g–h,3k–m), displaying the rapid effects of chronic stress on OPC dynamics. Interestingly, the OPC proliferation capacity on D6 (%Ki67$^+$ of PDGFRα$^+$) was significantly upregulated in SD-Sus and SD-Res compared to Con (Supplementary Fig. 3i–j). The increased proliferation of OPCs on D6 in response to chronic stress (Supplementary Fig. 3i–j) led to a significant increase of BrdU$^+$-labeled cells post-RSDS (Supplementary Fig. 2e). A significant percentage of these cells presented diluted BrdU$^+$ signal in the SD-Sus group (**weak BrdU$^+$ cells**; Supplementary Fig. 2g). Dilution of BrdU labeling could be the result of mitosis occurring post-BrdU administration and/or of OPCs asymmetric division. In support of the latter, many of these **weak BrdU$^+$** were differentiated OLN populations as illustrated in the SD-Sus

group on D15 (weakBrdU$^+$ PDGFRα$^-$; Supplementary Fig. 2h). This tendency for OPC transition into differentiated OLN stages (CSPG4$^-$Olig2$^+$) can also be observed in the early RSDS (D6; Supplementary Fig. 3n). These results suggest that the time-dependent rapid OPC proliferation in response to chronic stress may be followed by an upregulation of OLN progression.

Chronic stress induces the OPC differentiation into OLs in the mPFC.

To examine for potential alterations of OPC maturation, we administered BrdU *ad libitum* in the experimental groups to label the proliferating OPCs during RSDS and follow their lineage-progression post-RSDS (Fig. 2a–b). Histological analysis of *CSPG4*-EGFP$^+$ mice with the committed-OPC/immature-OL (C-OPC/Pre-OL) marker O4 and BrdU revealed a significant decrease of BrdU-retaining OPCs (% CSPG4$^+$O4$^-$ of BrdU$^+$), and a concomitant increase of C-OPCs (% CSPG4$^+$O4$^+$ of BrdU$^+$) and Pre-OLs (% CSPG4$^-$O4$^+$ of BrdU$^+$) in the SD-Sus compared to Con and SD-Res (Fig. 2c–f,2j). This led to significant increases of the O4$^+$ cell population and O4 protein levels (Supplementary Fig. 2i,2k–l) in the SD-Sus mice.

Downstream characterization of the OLN progression in the *CSPG4*-EGFP$^+$ mice, in combination with glutathione S-transferase-π (GST-π; OL) and BrdU resulted in significant increase of BrdU-retaining OLs in SD-Sus compared to Con and SD-Res groups (Fig. 2h,2j). Surprisingly, the overall upregulation of OPC differentiation did not yield increased OL density (GST-π$^+$) and GST-π levels (Fig. 2i, Supplementary Fig. 2k–l) in the SD-Sus mice. In contrast, the SD-Res mice exhibited a modest increase of both C-OPCs (O4$^+$), OLs (GST-π$^+$) and respective protein levels, compared to the Con (Fig. 2e,2i–j; Supplementary Fig. 2i,2k–l).

As reported, oligodendrogenesis can occur either through asymmetrical division or direct differentiation (without proliferation), with the former being rarely preferable, unless OPCs are responding to a homeostatic disturbance, such as cell death/injury or aberrant differentiation rates[2]. We utilized the *PDGFRα*-CreER^{T2}::*Rosa26*-EYFP mice to lineage-trace OPCs. In this system, after tamoxifen-induced (TMX) recombination eYFP is expressed in the OPCs (~73% recombination; **data not shown**). For induction of Cre-recombination, TMX was administered i.p. for 5 days[25], starting at P30. The RSDS paradigm was performed 1 month after the Cre induction (Supplementary Fig. 4a–b). The SD-Sus mice displayed a significant increase of the *PDGFRα::eYFP*$^+$ cells compared to Con and SD-Res, suggesting an increase of OPC proliferation earlier during RSDS (Supplementary Fig. 4c–d). A large portion of the eYFP-labeled cells in the SD-Sus mice were either C-OPCs/Pre-OLs (eYFP$^+$O4$^+$) or OLs (eYFP$^+$GST-π$^+$), compared to the Con and SD-Res groups (Supplementary Fig. 4e–i), depicting the dysregulation of the OLN progression following chronic stress (Supplementary Fig. 2j,2m).

Exposure to chronic stress induces myelin deficits post-RSDS.

Although the OL numbers were not altered in SD-Sus, we sought to investigate the OL myelin load. Myelin basic protein (MBP) analysis in *CSPG4*-EGFP$^+$ mice revealed striking deficits in the mPFC of SD-Sus mice, when compared to the Con and SD-Res mice

(Fig.3a,3c; Supplementary Fig. 2m; higher magnification). The deficits were confirmed by other classic myelin markers (CNP, MOG and MOBP; Fig. 3d,3e), suggesting that a large number of existing OLs could be dysfunctional. Oligodendroglial density (Olig2) was significantly decreased in the SD-Sus groups due to OPC losses (Fig. 3b; Supplementary Fig. 2k–l bottom panels). Decreased myelination and white matter (WM) deficits in MDD patients have also been reported for the ventral/lateral orbital cortices (VO/LO) and forceps minor (fmi)[26,27]. To that end, histological analysis of both areas post-RSDS revealed significant deficits of OPCs ($CSPG4^+$), OLs (GST-π^+), oligodendroglia ($Olig2^+$) and myelin density (MBP^+) in the SD-Sus mice compared to Con and SD-Res (Supplementary Fig. 5a–h).

Chronic stress induces OPC morphological impairments, excessive oxidative stress responses and OPC apoptosis in mPFC post-RSDS

OPCs are highly dynamic cells which continuously survey their local environment with multibranched processes, motile filopodia and extended growth cones[1,2], which are crucial for creating synaptic junctions with neurons (neuroglial junctions) and receiving neurotransmitter input[4,5]. We sought to characterize the OPC morphological features using Neurolucida hyperstacks acquired from the *CSPG4*-$EGFP^+$ mice. Remarkably, branched structural and Sholl analyses revealed significant reductions in OPC process intersection numbers, surface area and branch complexity in the SD-Sus mice compared to Con and SD-Res groups (Supplementary Fig. 6a–d; Supplementary Videos 1–3). Such OPC morphological alterations and extensive loss of process complexity have been previously related to OPC dysfunction, demyelination injuries, and apoptosis[2,28]. Therefore, we investigated the reactive oxidative species (ROS) production in the mPFC post-RSDS. We administered dihydroethidium (DHE) three hours before mouse euthanasia on D15, which interacts with superoxide radicals and produces red-fluorescent 2-hydroxyethidium (2-OH-E)[29,30]. Since microglia are a major source of ROS in CNS, we utilized the *CX3CR1*-GFP^+ reporter mice for histological analysis of 2-OH-E in OPCs ($PDGFR\alpha^+$) and microglia, revealing a significant upregulation of total ROS in the mPFC of SD-Sus mice (Supplementary Fig. 6e–f). ROS production was significantly increased in OPCs ($PDGFR\alpha^+$2-OH-E^+DAPI^+) and microglia ($CX3CR1^+$2-OH-E^+DAPI^+) in the SD-Sus mice compared to the Con and SD-Res (Supplementary Fig. 6g–h). Highest ROS production was reported by the microglial 2-OHE integrated density ($CX3CR1^+$2-OH-E^+DAPI^+)It is also important to note that microglial cell numbers were significantly increased in the SD-Sus groups (Supplementary Fig. 6i).

Differentiating oligodendroglia are considered vulnerable to ROS-related cytotoxic triggers resulting in OL deficits in cell numbers and myelin content[31,32]. To investigate if this is due to oligodendroglial apoptosis, we performed IHC in mPFC of *CSPG4*-$EGFP^+$ mice for cleaved Caspase-3 (Cl.Caspase3; apoptosis marker) and Olig2. Total Cl.Caspase3 levels were significantly higher in the OPCs/C-OPCs ($CSPG4^+Olig2^+Cl.Casp3^+DAPI^+$) of SD-Sus mice, compared to Con and SD-Res (Fig. 3g–h). Similar but less profound was the Cl.Casp3 increase in the Pre-OLs/OLs ($CSPG4^-Olig2^+Cl.Casp3^+DAPI^+$) of the SD-Sus mice (Fig. 3i). These results indicate that chronic stress can induce significant ROS production

and OPC structural atrophy in mPFC, contributing to aberrant OPC progression, leading potentially to oligodendroglial apoptosis.

Chronic stress triggers integrated-stress pathway responses and p-eIF2α/CHOP stimulation post-RSDS.

The integrated stress response (ISR) pathway plays a major role for the OLN progression, myelination, and cytoprotection during cellular stress stimuli (i.e., endoplasmic-reticulum stress, inflammation, ROS)[33]. The ISR is activated when the eukaryotic translation initiation factor eIF2α gets phosphorylated (p-eIF2α) and upregulates the activating transcription factor 4 (ATF4) to diminish global protein translation. However, should efforts to restore proteostasis fail and stress conditions persist, ATF4 can upregulate the C/EBP homologous protein (CHOP) transcription factor which induces cell apoptosis[34].

We investigated the D6 and D15 ISR responses of oligodendroglia following chronic stress. *CSPG4*-EGFP$^+$ mPFC sections were stained with p-eIF2α and Olig2 revealing a time-dependent activation of ISR (Supplementary Fig.7a–e). At D6, total and OPC-specific p-eIF2α (CSPG4$^+$p-eiF2α$^+$) significantly increased in the SD-Sus mice compared to Con and SD-Res, while the p-eIF2α expression in the SD-Res mice exhibited a modest increase compared to the Con (Supplementary Fig.7d–e). In contrast, total and OPC-specific p-eIF2α markedly decreased in the SD-Sus mice compared to Con at D15, while p-eIF2α in the SD-Res was considerably higher than the Con and SD-Sus mice (Supplementary Fig.7a–c).

We examined the downstream responses of ATF4 and CHOP in mPFC post RSDS. IHC analysis revealed remarkable upregulation of ATF4 in both SD-Sus and SD-Res compared to Con (Supplementary Fig.7f–h). This upregulation led to CHOP activation only in the SD-Sus mice as shown by the OPC-specific CHOP$^+$ and OPC-specific ATF4$^+$CHOP$^+$ expression in mPFC (Supplementary Fig.7i–k). These results suggest that chronic stress can drastically activate the ISR mechanism and potentially alter the homeostasis, fate, and function of oligodendroglia.

Long-term effects of chronic stress on OPC homeostasis in mPFC.

Considering that chronic stress and traumatic experiences display persisting effects on MDD-affected areas[35], we determined the long-term effects of chronic stress on oligodendroglial homeostasis and function. Following the RSDS paradigm and behavioral tests (BH1; D11-D14), mice were kept single-housed, and a 2nd round of behavioral tests was performed (BH2; D21-D24) (Supplementary Fig. 8a). The depressive-like phenotype of the SD-Sus mice persisted with ~80% of the SD mice displaying depressive-like phenotype, while the SD-Res (~20%) exhibiting only increased anxiety (Supplementary Fig. 8b,9a–e).

To examine the long-term effects (D25) of chronic stress on OPC homeostasis, proliferation capacity and lineage fate, we dual pulse labeled with BrdU (administered *ad libitum* during the RSDS paradigm) and three EdU doses at D17, D19 and D21 (Supplementary Fig. 8a). Histological analysis of mPFC confirmed sustained OPC losses in the SD-Sus mice, compared to Con and SD-Res (Supplementary Fig. 8c–d). In addition, the BrdU-retaining cells were considerably increased in the SD-Sus, while a large percentage of them displayed low BrdU intensity, due to OPC mitotic burst in the SD-Sus mice during early-RSDS

(Supplementary Fig.8e–g). Interestingly, only half of the BrdU-retaining cells were OPCs, indicating that the remainder has differentiated into Pre-OLs/OLs (Supplementary Fig. 6h). In addition, the proliferation capacity of the BrdU-retaining OPCs ($BrdU^+EdU^+PDFR\alpha^+$) was significantly lower in the SD-Sus mice (~10%) at D25, compared to the Con (~25%) and SD-Res (~28%) (Suppplementary Fig. 10i–j), and corresponding deficits in OPC proliferation were also confirmed by decreased $PDGFR\alpha^+Ki67^+$ expression at D25 (Supplementary Fig. 10a–d). Use of the mature OL marker (GST-π^+) revealed significant losses of mature OLs in the SD-Sus groups (Supplementary Fig. 10e–f) in mPFC, indicating that the aberrantly high OPC differentiation does not compensate for the OL reductions in D25 post-RSDS.

Single-nucleus transcriptomic characterization of oligodendroglial-lineage in the dlPFC of MDD patients.

To investigate whether our findings in RSDS rodent model may reflect the human condition, we utilized a publicly available dataset (Nagy et al., 2020[9]) of ~80,000 nuclear transcriptomes (sn-RNAseq) from the dorsolateral PFC (dlPFC) of MDD cases and psychiatrically healthy controls. Raw counts were downloaded from GEO (GSE144136) and expression objects were created using Seurat tool. Cell-type-specific, differentially expressed genes (DEGs) and OLN populations were identified, clustered using uniform manifold approximation and projection (UMAP), and annotated based on their expression of oligodendroglial-specific markers (*PCDH15, DSCAM, VCAN, SOX6, PDGFRα, CSPG4, OLIG2, OLIG1, CNTNAP2, CLDN11, CNP, PLP1, PCDH9, QKI, MBP, MOG, MAG*)[9,36]. Four common clusters (OPCs, C-OPCs, Pre-OLs, OLs; for Con and MDD) and an MDD-specific cluster (named Immune Oligodendrocytes; Im-OL, given that the cells expressed immune-related genes) were determined by the analysis (Fig. 4a). Pie charts with raw cell numbers from each cluster indicated alterations in the OLN progeny and reductions of the OL numbers (Fig. 4a). Dotplot analysis of the top expressed OLN population markers in Con and MDD patients revealed that the Im-OL cluster, along with the OL-specific gene signature, also expressed a range of immune-related components (Fig. 4b).

Immune oligodendrocytes, a distinct population with immune-related features, are altering the oligodenroglial-lineage in MDD patients.

The transcriptome profile of the Im-OL was examined using violin plots of marker genes shared in the OLN and Im-OL clusters as well as Im-OL characteristic DEGs, divided per condition (Fig. 4c). The Im-OL cluster exhibited a substantial expression of OLN-specific genes (keen to mature OLs), but also demonstrated a distinct phenotypic gene expression of immune-related genes *C3, HLA complex, P2RY12, ADAM28, DOCK8, LPAR6, ARHGAP24* (Fig. 4c). In addition, dot plot analysis and hierarchical clustering dendrogram of the top expressed OLN and microglial markers revealed that the immune-related gene signature of Im-OL was transcriptionally related to the microglial transcriptome cluster (Supplementary Fig. 11a). The double-faceted oligodendroglial/immune nature of Im-OL was further supported by heatmap analysis of their respective average gene expression, noting a significant correlation of Im-OL with both OLs (r=0.92) and Microglia (r=0.81) (Supplementary Fig. 11b).

To further characterize the role and functionality of Im-OL as part of the oligodendroglial-lineage, grouped gene scoring for myelin characteristic DEGs was used, divided per condition: *CNP, PLP1, PCDH9, QKI, MBP, MOG, MAG*. The MDD clusters exhibited significantly lower myelin gene scores compared to the respective Con clusters (Supplementary Fig. 11c). Importantly, the Im-OL cluster displayed a significant reduction of the myelin-related gene expression compared to the mature OLs, indicating myelination deficits or maturation arrest of OL-lineage during depression. In addition, gene set enrichment analysis of the top Im-OL markers identified a strong enrichment of Im-OL (p.adj.value<0.02) with genes involved in immune system processes and immune responses (Supplementary Fig. 11d), suggesting that the function Im-OL might be distinct than that of the other oligodendroglia.

Using the developmental-stage-specific OLN markers a predictive model of OLN pseudotime trajectory[37] was plotted: significant alterations in the progression of the OLN progeny in MDD samples were observed. With starting point the OPC cluster (R; root), the control (Con) patient trajectory exhibited the traditional lineage progression: OPC → C-OPC → Pre-OL → OL. The MDD patient trajectory revealed two alternate routes of cell fate commitment, either toward OLs through the Im-OL population, or toward pre-OLs, with the latter suggesting myelination arrest of OLs (Fig. 4d). In addition, colocalization plots of key oligodendroglial markers (*PDGFRa, CSPG4, CLDN11, PCDH9, PLP, MBP*) with characteristic Im-OL markers showed that the Im-OLs are transcriptionally closer to the Pre-OL/OL cluster (Supplementary Figs. 15–17), supporting the pseudotime trajectory of the oligodendroglia in MDD patients.

Oligodendroglial expression of MHCII, complement C3 and P2RY12 in the RSDS-affected areas.

Based on the top Im-OL expressed DEGs (*HLA complex, C3* and *P2RY12*) in MDD patients (Fig. 4c), we examined this novel oligodendroglial subset of Im-OL in the RSDS model using the MHCII, C3 and P2RY12 markers. Histological analysis of *CSPG4*-EGFP$^+$ mice, co-stained with O4 (C-OPCs/Pre-OL) and MHC class II (I-A/I-E) antigen presentation markers revealed a significant expression of MHCII by oligodendroglia in the SD-Sus mice, compared to the Con and SD-Res (CSPG4$^-$O4$^+$MHCII$^+$) (Fig. 5a–e). Among these populations, the Pre-OLs exhibited the largest percentage of total MHCII in mPFC, which agrees with the bioinformatic analysis of the Im-OL cluster. Analogous expression was observed by histological analysis of *CSPG4*-EGFP$^+$ mice with O4 and complement C3 markers, revealing a significant upregulation of C3 expression in the oligodendroglia of SD-Sus mice at mPFC, and most specifically by the Pre-OL lineage-stage (CSPG4$^-$O4$^+$C3$^+$) (Fig. 5f–j). For both MHCII and C3 the Pre-OLs of the SD-Res mice exhibited a modest, but significant increase compared to the Con. MHCII and C3 expression in the adjacent areas of VO/LO and fmi were also significantly increased in the SD-Sus mice, compared to Con and SD-Res (Supplementary Fig. 12a–p). *P2RY12*, encodes the microglial marker purinoceptor 12 (P2RY12)[38]. Its expression is reported to be downregulated during inflammatory responses and stress conditions (M1-like microglial activation)[39]. P2RY12 expression levels in mPFC were significantly decreased in the SD-Sus mice compared to Con and SD-Res groups (Supplementary Fig. 13g–h). Remarkably, in proximity with

the microglial cells (P2RY12^{+}), P2RY12 was also localized in OLN populations and significantly upregulated in the SD-Sus groups (most predominantly in Pre-OL stage; CSPG4^{-}O4^{+}P2RY12^{+}) (Supplementary Fig. 13i–k). Overall, we validated the existence of OLN cells which express immune genes in the RSDS mouse model, analogous to the top markers expressed in Im-OL population in the MDD patient cohorts.

Oligodendroglial expression of MHCII in mPFC mediates microglial phagocytosis of myelin elements

Microglia are important antigen-presenting cells in CNS that get activated in a MHCII-dependent manner during neurodegeneration[40]. Recent evidence from Multiple Sclerosis studies have suggested similar roles for OLN cells, including antigen presentation and direct communication and recruitment of innate and adaptive immune cells[41,42]. These observations suggest that Im-OL may act as mediators of immune responses. We investigated whether Im-OL play a similar role in the RSDS model. We performed IHC in *CX3CR1*-GFP^{+} mice for CNP (myelin marker) and MHCII to evaluate microglial phagocytosis of myelin. Microglial expression of MHCII and dramatic myelin deficits (CNP) were evident in the mPFC of SD-Sus mice (Supplementary Fig. 13a–c), where a significant percentage of CNP co-localized with MHCII (~12%), compared to the Con and SD-Res groups (Supplementary Fig. 13a,d). Focusing on myelin phagocytosis by microglia (CX3CR1^{+}CNP^{+}), both SD-Sus (~8.5%) and SD-Res (~7.5%) displayed a significant increase compared to Con (~6%), however almost half of the myelin sheath in the SD-Sus mice was “tagged” with the MHCII (~4%; CX3CR1^{+}CNP^{+}MHCII^{+}), compared to the Con (<1%) and SD-Res (~1%) groups (Supplementary Fig. 13e–f), suggesting an antigen presentation role for Im-OL in response to chronic stress.

Discussion

In this study we demonstrated that chronic psychosocial stress disrupts the OPC homeostasis, oligodendroglia-lineage progression and causes severe myelin deficits, associating a novel population of immune oligodendrocytes with depressive-like behavior (Supplementary Fig. 14). We employed the RSDS paradigm, a well-established mouse model of depression[24], to elucidate the cellular dynamics and molecular mechanisms of these perturbations. In line with previous studies[8,24], the majority of SD mice displayed long-lasting depression-like features (SD-Sus; social aversion, stress/anxiety, anhedonia, despair), while a smaller cohort exhibited resilience to stress (SD-Res), reflecting the heterogeneous responses to chronic stress in the human population[43]. We observed that chronic stress can lead to major OPC population losses in the mPFC of SD-Sus mice (D6), which can persist for several weeks after the end of the paradigm (D25). The results agree with previous findings reporting significant OPC reductions in the mPFC of depressive-like rodents and MDD patients[8,44]. These effects did not reflect a generalized response to chronic stress, since OPC density was not altered in areas not involved in the MDD pathophysiology (somatosensory and motor cortices; data not shown).

Despite the dramatic OPC losses, chronic stress led to a transient proliferation surge of OPCs in the SD-Sus mice after miniSD (D6), which was followed by sustained reductions

of OPC proliferation post-RSDS in mPFC (D15). The initial proliferative surge of OPCs could reflect a regulatory effort to restore their cell density[2], or a response to OL/myelin deficits and concomitant neuronal activity changes, as reported in the mPFC of MDD patients and depression animal models[14,20,35]. Tracing the oligodendroglial-lineage fate by BrdU-labeling or *PDGFRα::eYFP*$^{+}$ recombination revealed that the initial proliferative response by OPCs was followed by increased differentiation into C-OPCs and Pre-OLs in the mPFC of SD-Sus mice. In addition, the dual-pulse labeling of OPCs indicated that the aberrant differentiation rates and diminished proliferation persisted for at least 2 weeks post-RSDS (D25), evidence for long-term OLN deficits in the mPFC response to chronic psychosocial stress. Notably, the amplified OPC differentiation did not translate into an increase of myelinating OLs post-RSDS (D15) but rather to a significant decrease on D25, suggesting that these OPCs may have differentiated but failed to fully mature. This is further supported by the OL myelin deficits identified in the mPFC in our study, as well as in previous animal[13,14] and clinical[17] studies. Myelin deficits and alterations in OLN-lineage were also reported in the VO/LO and fmi areas, which are associated with WM deficits observed in MDD patients[26,27]. In contrast to the significant compromises of OLN homeostasis in the SD-Sus groups, the SD-Res mice demonstrated increased OL density (GST-π^{+} cells), intact myelin content and low OLN cell apoptotic rates. These observations along with the increased OPC proliferation at the early (D6) and later stages (D15) of RSDS and the modest increase in OLN-progeny progression further strengthen the physiological association of OLN homeostasis with the depressive-like pathophenotypic behavior[1,8,9].

Previous studies have established that radial morphological features in OPCs associate with reception of direct synaptic input and response to neuronal activity changes[45,46]. Here, we revealed dramatic alterations of OPC morphology after chronic stress, suggesting disruption of neuro-glial communication. Similar atrophic-like OPC features have been previously reported in demyelinating/inflammatory conditions, oxidative stress, and cell apoptotic events[2,13,28].

Consistent with previous studies implicating neuroinflammation and oxidative stress during depression[30,47–49], we detected an upregulation of microglial ROS production and significant microglial recruitment in SD-Sus mice. The SD-Sus mice also displayed a substantial increase of OPC-specific ROS production, indicative of oligodendroglial dysfunction post-RSDS. OPCs are vulnerable to sustained oxidative stress [31] due to their high metabolic rate and the extensive protein synthesis needed for OL myelin production [50]. ROS production can trigger expression of key members of the ISR pathway by depleting the antioxidant defense machinery in OPCs [51], suggesting that ISR plays a major homeostatic role in the translational control of OLN progression (proteostasis), myelination, and cytoprotection from stress stimuli[33,34]. Analysis of the ISR mechanism in the SD-Sus mice revealed that chronic stress supports a transient induction of OPC-specific p-eIF2α on Day6, which was downregulated on Day15. The initial upregulation of p-eIF2α was sufficient to promote a sustained induction of ATF4, leading to CHOP activation on D15. However, when cellular stress remains unmitigated, the protective abilities of the ISR are overwhelmed, inducing the accumulation of the proapoptotic protein CHOP, subsequently leading to apoptosis[33]. Additionally, CHOP induction can result in dephosphorylation of p-eIF2α, as a feedback mechanism, through the GADD34-dependent protein phosphatase

1 (PP1)[52]. The latter, along with the significant loss of OPCs on D15 (normally major contributors of the total p-eIF2α), could explain the p-eIF2α reduction observed on D15. In contrast, the moderate activation of the OPC-specific p-eIF2α and ATF4 did not result in ISR exhaustion or CHOP induction in the SD-Res groups, suggesting that manipulation of the ISR mechanism could potentially protect the fate and homeostatic function of oligodendroglia[53]. Both ROS and ISR pathways have been shown to converge upon their sustained activation into caspase-related apoptotic signals and pro-apoptotic events[50]. ATF-4 co-operates with CHOP to induce death in cells overproducing ROS as a corollary to increased rates of protein synthesis and a malfunctional protein folding machinery[54]. In support of that, significant OPC and OL apoptosis was evident in the SD-Sus mice post-RSDS, as a consequence of the sustained malfunction of the ISR machinery and ROS elements after chronic psychosocial stress. Utilizing a sn-RNAseq dataset from the dlPFC of MDD patients[9], we identified a novel OL MDD-specific population, recently described in multiple sclerosis (MS) patients[36], the Immune OLs. Im-OL expressed both characteristic-OL genes as well as several immune-related factors involved in processes and responses usually associated with immune cells (such as microglia). The Im-OL molecular signature we determined was highly correlated with the Im-OL population from MS patients[36] (Supplementary Fig. 20). Significantly, a pseudotime trajectory of OPCs revealed an aberrant OLN progression in the MDD patients due to the substantial Im-OL myelin gene-expression deficits, which further supports our hypothesis for disturbances in the OL-lineage and OL-maturation arrest.

Based on the top-expressed genes of the Im-OL cluster, we demonstrated that oligodendroglia (predominantly pre-OLs and OLs) from several depression-affected areas significantly expressed the immune-related components: MHCII, C3, P2RY12, in the SD-Sus mice. In previous studies with MS patient samples and in diabetic animals, it was demonstrated that interferon-γ could induce expression of MHCII[55], and modify the expression of P2RY12[56]. It would be interesting to examine whether interferon-γ, potentially secreted by microglia is responsible of the upregulation of these immune-related genes in the context of RSRS, the induction of ISR, and the differentiation of OPCs towards Im-OL. The interaction of Im-OL with microglia suggests that Im-OL may mediate microglial phagocytosis of myelin elements. To that end, recent reports note that immune-related OLs function as antigen-presenting cells and instigate immune cell recruitment in MS[41,42,57]. These findings further support the hypothesis that Im-OL could serve as a “tagging” homeostatic mechanism for clearance of dysfunctional oligodendroglia during stressful or inflammatory conditions, emerging as active immune mediators. Further phenotypic, and functional characterization of these populations is crucial to better understand the role of Im-OL in CNS homeostasis and neuropsychiatric disorders.

Material & Methods

Animals

All animal procedures were approved by the Institutional Animal Care and Use Committee (covered by Animal welfare assurance No A3011-0), Renaissance School of Medicine at Stony Brook University, and conducted in accordance with the guidelines of the National

Institutes of Health “Guide for the Care and Use of Laboratory Animals”. Experiments were performed using adult (2–3 months old) male mice [C57BL/6J (wt), *CSPG4*-EGFP (Jackson Labs, 022735 model FVB.Cg-Tg(Cspg4-EGFP*) HDbe/J), *CX3CR1*-GFP (Jackson Labs, 005582 model B6.129P-Cx3cr1tm1Litt/J), *PDGFRα*-CreERT2 (Tg(Pdgfra-cre/ERT2)1Wdr; from[58]), *Rosa26*-EYFP (Jackson Labs, 006148 model B6.129X1-Gt(ROSA)26Sortm1(EYFP) Cos/J)] were used wherever mentioned. All the mouse lines were backcrossed to a C57BL/6J background, bred in-house, and genotyped by PCR. CD-1 retired-breeder male mice (Charles River Laboratories, CD-1 IGS mice, strain code:022) were used as aggressors. For induction of recombination in the *PDGFRα*-CreERT2 :: *Rosa26*-EYFP mice, tamoxifen (Sigma CAS # 10540-29-1) dissolved in ethanol : sunflower seed oil was injected intraperitoneally (i.p.) starting at P30, at a daily dose of 75 μg/g body weight (from a 10 mg/ml stock), for 5 consecutive days, as in[25]. All animals were housed in 12-h light/dark cycle. Food and water were provided *ad libitum* by the experimenters.

Repeated social defeat stress paradigm (RSDS)

Adult male mice were subjected to repeated bouts of physical aggression (“defeats”) from aggressive CD-1 mice for 10 consecutive days, as previously described[8,24]. The CD-1 aggressors were screened during a 3-day screening period for adequate aggressive behavior and then housed on one side of the divided mouse cage (known as the home cage), at least overnight prior to the start of defeat sessions. All defeat experiments were performed within that compartment, while the intruders were rotated across defeat days, so that the experimental animals would not habituate to a single aggressor. On day 0 (D0) of RSDS the ‘socially defeated-to be’ (SD) mice were placed into the aggressor’s space for 10 min (physical stress), and after the end of the encounter they were returned to their side overnight. The mice could see and smell the aggressor through the clear perforated divider (sensory stress). The naïve mice were exposed to wt (C57BL/6J) mice, instead, for 1 minute. About 80% of the mice that were subjected to social defeat stress displayed depressive-like behavior (SD-Sus for Susceptible), whereas the rest 20% were the nonresponding mice (SD-Res for Resilient) did not, thus modeling the heterogeneity in individual responses to stress in humans[59]. At the end of RSDS paradigms all animals were singly housed. Socially defeated mice were categorized based on the SI output, and further behavioral analyses for each group followed this categorization. Both SD-Sus and SD-Res exhibited anxiety-like behavior, however the SD-Sus additionally demonstrated social avoidance, reduction of reward under stress, anhedonia, despair-like behavior, and elevated plasma corticosterone levels (~130 ng/ml)[59]. In addition to this paradigm, a shorter adaptation (3 days social defeat) was also used in this study.

Behavioral analyses

For endpoints D15 and D25, mice were behaviorally tested for 4 days (1 experiment/day), while for endpoint D6, mice were tested for 3 days (1 experiment/day) prior to euthanasia. Behavioral testing and recordings were performed during the light phase. Both naïve and SD mouse groups were tested for behavioral alterations using the i) social interaction test (SI; measures social avoidance), ii) elevated plus-maze test (EPM; measures stress/anxiety), iii) forced swimming test (FST; measures despair-like behavior), iv) sucrose preference test (SPT; assesses anhedonia-lack of feeling pleasure), and v) novelty suppressed feeding test

(NSF; assesses reward under stress). All experiments (except for SPT) were performed in a light-controlled and sound-isolated behavioral analysis room. The mice were acclimatized to the experimental room for 1 hour before the start of each experiment. The SI and EPM were performed under red light conditions; the remaining behavioral tests were performed with lights on. The software Noldus Ethovision XT16 was used for the automated tracking and scoring during the behavioral tests. White noise generator (70–75 dB) was used to mask intermittent disturbing sounds (from surrounding areas) that would potentially startle the animals.

Social Interaction (SI)—One day after the final social defeat stress interaction, a SI test was performed to determine whether the animals display social avoidance, as previously established[24]. Mice were placed into the social interaction open-field arena [(42 cm (w) × 42 cm (d) × 42 cm (h)], and the time spent in the interaction zone (<8 cm from the wire-mesh enclosure) was monitored for the two 2.5-min phases (without or with a novel CD-1 aggressor present in the enclosure), separated by a duration of 30 s. The socially defeated mice with SI ratio [(Time in interaction zone with aggressor) / (Time in interaction zone without aggressor)] >1, were classified as SD-Res and mice with a ratio below 1 (social avoidance), were classified as SD-Sus[8]. The naïve mice were categorized as Control (C).

Elevated plus-maze test (EPM)—The apparatus used for this test was cross-shaped with two open arms (30 cm × 5 cm) and two closed arms (30 cm × 5 cm × 15 cm) that extended from a central platform (5 cm × 5 cm), as previously[8,60]. The entire maze was elevated 40 cm above the floor. The enclosed arms offered safety when the mouse was stressed; on the other hand, the open arms offered the motive of exploration. Each mouse was placed in the central square of the apparatus, facing an enclosed arm. The mice were let to roam freely for 10 min totally; an arm entry was defined when all four paws entered an arm. The total mobility, time spent in open arms and time closed arms were recorded, as an index of stress/anxiety[60].

Forced swimming test (FSM)—Each mouse was placed in a transparent tank [inescapable Plexiglas cylindrical tank (height: 30 cm, diameter: 22.5 cm)] that was filled with water (to a depth of 15 cm and maintained at 25 °C) and their escape related mobility behavior was measured. Once the mouse was in the water, it was left to swim for 6 min in total, assessing the behavior only during the last 4 min, as previously performed[61–63]. The mice that acquired an immobile posture, characterized by motionless floating in the water, were termed immobile (immobility time), making only the necessary movements to keep the head above the water. Before returning the animals to their home cages, they were dried gently using paper towels to prevent hypothermia.

Sucrose preference test (SPT)—The SPT was performed as previously with slight modifications[8,64]. The experimental groups were habituated for 72 h to 2% sucrose, in which the bottles were alternated to avoid bias for a specific cage side. The day before the testing the mice underwent an 18 h water deprivation period. The day of the testing bottles filled with sucrose 2% or water were weighed, and consumption was determined for a 24 h period. Bottles were weighed again at the end of the 24 h period. Sucrose preference was

expressed as (Δweightsucrose) / Δweightsucrose + Δweightwater) x100. Sucrose preference score less than 70% was displaying anhedonia.

Novelty suppressed feeding test (NSF)—The NSF test measures the time that mice take to approach and eat food in a novel environment following an extended period of food deprivation. Mice were food-deprived for 24 h and moved in freshly prepared home-cages (to avoid any pellets remaining on the bedding). The next day, each mouse was placed at the corner of an open-field arena [(42 cm (w) × 42 cm (d) × 42 cm (h)] and a pellet of chow was already positioned at the center of it. The time until the first bite of the chow pellet was recorded, with maximum trial time the 10 min. After the trial, the mice were returned to their home cage which contained a pre-weighed food pellet, and food consumption was measured for a period of 5 min, as described[65,66].

Plasma corticosterone levels

Blood samples were collected from the animals before the euthanasia, unless stated otherwise. The subjects were anesthetized by isoflurane, and they were placed in a restrainer (for easier extraction). The tail was warmed with a red light and snipped by a scalpel blade. Blood samples were collected (~100 μl) into lithium-heparin collection tubes (BD Vacutainer® tubes, 265729). Plasma was separated from whole blood by centrifugation and was stored at −80°C, until use. For measurement of plasma corticosterone levels, the samples were diluted 1:40 in buffer and measured using the Corticosterone EIA kit (Enzo Life Sciences, ADI-900-097), according to the manufacturer's instructions.

BrdU and EdU labeling

For the labeling of proliferating cells, 5-Bromo-2′-deoxyuridine (BrdU;Sigma-B5022) was dissolved in drinking water (1 mg/ml), and all mouse groups were given access to the water *ad libitum* throughout the 10 days of the RSDS paradigm[8]. For dual-pulse labeling of proliferating populations, 5-ethyl-2'-deoxyuridine (EdU; ThermoFisher Scientific -E10187) was administered i.p. at D17, D19 and D21 (x3 at D17, D19, D21) at a dose of 100 μg/g body weight (8 mg/ml EdU in 0.9 % NaCl), as in[67].

Reactive oxygen species (ROS) measurement

For the *in-situ* detection of oxidative stress in the form of ROS production, dihydroethidium (DHE; #D1148, ThermoFisher Scientific) was dissolved at 2 mg/ml in 100% DMSO, and then diluted 1:1 with sterile saline to 1 mg/ml. Three hours before euthanasia, the subjects were i.p. administered a DHE dose of 10 μg/g body weight, as previously described[29]. DHE is a redox-sensitive probe, which is oxidized by superoxide radicals to ethidium[68], generating the highly superoxide-specific, red fluorescent product 2-hydroxyethidium (2-OH-E), which intercalates within the DNA. The excitation (Ex) and emission (Em) wavelengths used for the 2-OH-E were 405 nm and 580–620 nm respectively, to preferentially detect emissions from 2-OH-E and avoid nonspecific detection of ethidium (nonspecific product of DHE oxidation), as previously[30,69].

Immunoblot analysis

Mouse subjects were euthanized with isoflurane overdose, and freshly extracted brains were micro-dissected using a McIlwain tissue chopper to obtain ~500-μm thick brain coronal sections. Medial PFC was dissected out (with the help of a dissecting microscope) from +1.2 mm to +2.5 mm anterior to bregma slices. Protein lysate was prepared using RIPA buffer (120–150 μl) with protease and phosphatase inhibitors (200 mM PMSF, 100 mM sodium orthovanadate, and protease inhibitor cocktail; Santa Cruz, sc-24948A). Lysates were shaken for 15 min at 4 °C, cleared by centrifugation at 15,000 g for 10 min at 4°C, and protein concentration was determined using the Pierce BCA Protein Assay Kit (ThermoFisher Scientific; 23225). Samples (15–20 μg) were boiled for 5 min with 5X SDS-PAGE sample loading buffer (Thermo Fisher Scientific; 39000), separated by SDS-PAGE, and transferred to PVDF membranes (ThermoFisher Scientific; 88518) at 30 V for 16–18 h at 4°C. Membranes were blocked with 5% w/v nonfat dry milk (Cell Signal; 9999S) and incubated with primary antibodies (Supplementary Table 2a) for 16–18 h at 4°C. Washes with TBST (Cell Signal; 9997S) were followed by incubation with HRP-coupled secondary antibodies (Supplementary Table 2b). Signal was visualized by Sapphire Biomolecular Imager (Azure Biosystems) using a chemiluminescent substrate mixture (Supersignal West Pico Plus; ThermoFisher Scientific, 34580 or Immobilon Western; Millipore, WBKLS0500). Optical densities were collected with Fiji ImageJ software[70]. Where indicated, protein levels were expressed as fold change (versus Control) of the arbitrary units (A.U.) following normalization to the corresponding loading controls (β-Actin, GAPDH). Samples were normalized to the total protein for each sample, as determined by the BCA assay. For detailed antibody list used see Supplementary Table 2a.

Immunohistochemistry

Deeply anesthetized mice were transcardially perfused with cold 1X PBS (15 ml) followed by cold PFA fixative solution (4% paraformaldehyde in 1X PBS; 20ml) and brains were dissected and post-fixed for an additional 24 hours. Then brains were cryoprotected in 30% sucrose for 24 hours and sectioned with a sliding microtome. Free-floating brain sections (30–40 μm thick) containing the mPFC, VO, LO and fmi were blocked with 10% goat serum (ThermoFisher Scientific; 16210072) in 0.3% TritonX-100 in 1X PBS for 1–2 hour at room temperature. Tissue sections were incubated with primary antibodies overnight at 4°C at the indicated concentrations (Supplementary Table 2a). The following day, sections were washed in PBS-Triton and incubated with the appropriate cross-absorbed secondary antibodies (Supplementary Table 2c). After 4 additional washes nuclei were stained with DAPI (Sigma; D9542) and sections were mounted using MOWIOL mounting media. For BrdU IHC, sections were pretreated in 2M HCl for 40 minutes at 37°C, followed by 2–3× 5-minute washes in 0.1 M Boric acid (pH 8.5). For BrdU and EdU double staining, tissue was processed for BrdU and followed by EdU labeling with Click-iT Plus EdU Cell Proliferation Kit-Alexa Fluor 555 (ThermoFisher Scientific, C10638), according to the manufacturer's instructions. For detailed antibody list used see Supplementary Table 2a.

Microscopy and histological quantification

The confocal laser-scanning microscopes Leica TCS SP8X and Leica TCS-SP5 were used for imaging of FITC, EGFP, EYFP, Alexa-488, Alexa-555, Alexa-594, Alexa-647, 2-OH-E and CY3 fluorophores. Optical sections (z = 1.0μm; total stack of 10–16μm for 1 cell layer) of confocal epifluorescence images were sequentially acquired using 10x, 20x, 40x (N.A. 1.30), 63x (N.A. 1.20) and 100x (N.A. 1.40) objectives, with LAS AF software. Fiji ImageJ software[70] was used for image reconstruction, cell counting, integrated density analysis and colocalization analysis. For mPFC analysis, 6 fields (located between +1.2mm to +2.5mm anterior to bregma), containing the cingulate cortex (Cg1), prelimbic (PL), infralimbic (IL) and medial orbital cortex (MO) were taken from each animal, for quantitative analysis. For VO/LO analysis, 4 fields (located between +2.0mm to +2.5mm anterior to bregma), containing the ventral orbital cortex (VO), and lateral orbital cortex (LO), were taken from each animal for quantitative analysis. For fmi analysis, 3 fields (located between +1.2mm to +1.7mm anterior to bregma), containing the forceps minor (fmi), were taken from each animal for quantitative analysis. Typically, 3–4 brain slices were analyzed per animal, and at least 3 different animals for each experimental condition were evaluated. Cell counts were presented as the number of marker$^+$ cells/section (section corresponding to 0.2mm^2). Each section quantification depicts the sum of the marker$^+$ cells from all the analyzed fields. For the integrated density analysis, the IsoData thresholding was applied to each image, and the integrated density [is defined as the product of pixel intensity (255 = the maximum pixel intensity for an 8-bit image) × area] was measured. For the colocalization analysis, the IsoData thresholding was applied to each image, images were merged, compartmentalized, and the integrated density was measured for the colocalized signal. Each section with integrated density quantification is depicted by the mean of the integrated density from all the analyzed fields. Additionally, for the analysis of weak BrdU$^+$ cells the low threshold level was set at 120. Any cells not observable at that threshold were termed as weak-labeled BrdU$^+$ cells, depicting the diluted labeling cells after several proliferation cycles[71]. All experimental group comparisons were conducted on sections stained and imaged with identical exposure and acquisition settings. All analyses were performed on raw images, prior to any image processing by Adobe Illustrator CS6 for representation purposes. The cell counting was performed in a blinded manner by 4 experimenters collectively, and tissue sections were matched across samples.

Glial morphological analysis

To quantitatively examine OPC morphology, unprocessed 30μm z-stack confocal images (100x objective; 20 individual images, step size: 1.5μm) of cells for *CSPG*-EGFP activity in the mPFC area were imported into Neurolucida software, as previously described[3,72]. Cell bodies and processes were manually traced (6 cells/mouse), and a 3D rendering was created. The 3D reconstructions were imported into Neurolucida Explorer for branched structure analysis and Sholl analysis (10μm starting radius, 80μm ending radius, and 10μm step size). Number of process intersections, cell surface area, and cell complexity were measured. OPC complexity = [Sum of the terminal orders + Number of terminals] * [Total dendritic length / Number of primary dendrites]. Terminal orders: Number of “sister” branches encountered as proceeding from the terminal to the cell body (calculated for each terminal); Terminal: Refers to process endings.

Bioinformatic Analysis of Publicly Available Dataset

snRNAseq—Raw counts were downloaded from GEO (GSE144136) from Nagy et al.,[9], and expression objects were created using Seurat[73,74]. Quality control (QC) was performed, and cells with abnormally high or low feature counts and percent mitochondrial gene expression ≤2% were removed. Using the WhichCells() function (Seurat) OLN cells were subsetted based on their expression of oligo-specific markers (*PCDH15, DSCAM, VCAN, SOX6, PDGFRα, CSPG4, CLDN11, CNP, PLP1, PCDH9, QKI, MBP, MOG, MAG*).

Oligodendroglial-Lineage Classification

To visualize discrepancies between conditions in oligodendroglial cells, the new expression object was subset by condition (MDD and Control) and the following hyperparameters were used to run UMAP on the two new objects: n.neighbors = 20, min.dist = 0.2. Four similar clusters and one MDD-specific cluster resulted from the analysis. The distinct clusters were labeled based on their expression of OPC and Committed OPC (*PCDH15, DSCAM, VCAN, SOX6, PDGFRα, CSPG4, OLIG1, OLIG2),* and Immature Pre-myelinating and Mature Myelinating Oligodendrocyte (*CNTNAP2, CLDN11, CNP, PLP1, PCDH9, QKI, MBP, MOG, MAG*) markers. The one unique MDD cluster was labeled Immune Oligodendrocytes (Im-OL), based on their expression of immune markers (*P2RY12, CD74, C3, ITGAX, ITPR2, ARHGAP24, ADAM28, LPAR6*).

Grouped Violin and Dotplots—To visualize the gene expression of early and late oligodendroglia as a whole, we grouped the OPC and Committed OPC clusters (termed OPCs), and the Immature Pre-Myelinating OL and Mature Myelinating OL clusters (termed OLs). Using the WhichCells() function, we defined which cells belonged to the four initial clusters and then re-labeled them using the SetIdent function. The Violin plots and Dotplots were then created using the standard Seurat functions. Dotplots displaying a hierarchical clustering were also created using the standard Seurat function. To perform this hierarchical clustering, after grouping the cells (as mentioned above) the object underwent a pseudobulking technique in which we averaged the counts for each of the labeled cell types. This new matrix was then cleared of missing values and fed into the hclust() function which performed the hierarchical clustering and visualized with as dendrogram() cluster.

Integration with published dataset—To verify the cluster labeling, and the credibility of our immune oligodendrocytes cluster, our oligodendrocyte object was integrated with those published by Jäkel et al, 2019[36] using Seurat's integration and label transfer method. Raw counts for the Jäkel data were downloaded from GEO (GSE118257)[36], and expression objects were created using Seurat. In preparation for the integration, we subset the oligodendroglia based on the Jäkel labels. The two objects were then integrated and a pseudobulking method was applied, in which we averaged the counts across each of our and Jäkel's labeled cell types. We then computed the correlation coefficient between samples (clusters) using the Cor() function and plotted a heatmap using the pheatmap() function[75].

Comparison with Microglia—Given that the Im-OL cluster displays several immune components, we sought to compare it to the innate immune cells, microglia. To do so, we subsetted OL lineage cells and microglia from the originally read in object and again

pseudobulked the cell clusters. The correlation coefficient between samples (clusters) was then computed using the Cor() function and a heatmap plotted using the pheatmap() function.

Pseudotime Analysis—The two separated Seurat objects (MDD and Control) were used for the Pseudotime analysis. Separately, the UMAP coordinates and feature loadings for each object were passed to Monocle3 and pseudotime graph was learned using default parameters[37,76].

Gene Scoring—A Gene Scoring technique was used to calculate a Gene Signature "Score" for each of the OLN clusters. First, a signature containing the genes of interest was created. The raw counts were then extracted from the Seurat object and log normalization was performed. We then averaged the log normalized counts for each of the genes in the signature. For the HLA gene complex (*HLA-A, HLA-DPA1, HLA-DRB1, HLA-DQB1, HLA-C, HLA-DPB1, HLA-DOB, HLA-DRB5, HLA-DQB2, HLA-B, CD74*), signature "score" was added back into the Seurat object metadata and plotted using the VlnPlot() function. For the myelin gene scoring (*CNP, PLP1, PCDH9, QKI, MBP, MOG, MAG*), column statistics were performed.

Gene Set Enrichment Analysis

To conduct the gene set enrichment analysis (GSEA) for the Im-OL cluster, the Seurat FindMarkers() function was utilized to attain the genes that were differentially expressed (DE) in the Im-OL cluster versus the other OL clusters. The DE genes were ranked using the following function: sign(average- log2Fold-Change) × −log10(p-value). The ranked gene list was then fed into the gseGO() function of the clusterProfiler package[77], using "Biological Processes" as the ontology. The plot was made using the standard clusterProfiler functions.

Colocalization plots—To visualize the colocalization of OLN and Im-OL characteristic genes within the ImOL cluster, the cluster was first subsetted from the rest of the object. After re-running standard clustering parameters, the FeaturePlot function from Seurat was used with the following hyperparameters: Blend = TRUE.

Statistical analysis

No statistical methods were used to predetermine sample size *a priori*, but the sample sizes used were similar to those reported in[8]. Furthermore, representative data from each experiment were examined by Shapiro-Wilk's test ($p>0.05$)[78] and a visual inspection of their histograms to confirm normal data distribution[79,80]. The majority of the experimental analyses was performed by parametric ordinary one-way analysis of variance (ANOVA), followed by Tukey's multiple comparison post-hoc tests. For the glial morphological analyses two-way ANOVA was performed, followed by Tukey's multiple comparison post-hoc tests. For the myelin DEG scoring analyses, one-way Kruskal-Wallis analysis was performed, followed by Dunn's multiple comparisons test. The GraphPad Prism 8 and Excel (Microsoft) were used for all statistical analyses, except for the Bioinformatic Analyses (R-Studio). The data were reported as mean ± S.D. with symbols indicating the following P value ranges: *$P \leq 0.05$, ** $P \leq 0.01$, *** $P \leq 0.001$ and **** $P \leq 0.0001$).

Supplementary Material

Refer to Web version on PubMed Central for supplementary material.

Acknowledgements

We are grateful to Dr. Antonis E. Koromilas for providing reagents and insightful discussion on the manuscript. We also thank Drs. Ramin Parsey, Christine DeLorenzo, Joel Levine and Holly Colognato for their valuable insight and discussions. This work was supported by the National Institute of Mental Health, Grant/Award Numbers: R01MH123093-01, R01MH123093-01S1 (MMM), the American Heart Association (19PRE34370044; AGK) and Scholars in BioMedical Sciences Program (T32GM127253).

References

1. Birey F, Kokkosis AG & Aguirre A Oligodendroglia-lineage cells in brain plasticity, homeostasis and psychiatric disorders. Current opinion in neurobiology 47, 93–103, doi:10.1016/j.conb.2017.09.016 (2017). [PubMed: 29073529]
2. Hughes EG, Kang SH, Fukaya M & Bergles DE Oligodendrocyte progenitors balance growth with self-repulsion to achieve homeostasis in the adult brain. Nature neuroscience 16, 668–676, doi:10.1038/nn.3390 (2013). [PubMed: 23624515]
3. Birey F & Aguirre A Age-Dependent Netrin-1 Signaling Regulates NG2+ Glial Cell Spatial Homeostasis in Normal Adult Gray Matter. The Journal of neuroscience : the official journal of the Society for Neuroscience 35, 6946–6951, doi:10.1523/jneurosci.0356-15.2015 (2015). [PubMed: 25926469]
4. Bergles DE, Roberts JD, Somogyi P & Jahr CE Glutamatergic synapses on oligodendrocyte precursor cells in the hippocampus. Nature 405, 187–191, doi:10.1038/35012083 (2000). [PubMed: 10821275]
5. Doyle S, Hansen DB, Vella J, Bond P, Harper G, Zammit C et al. Vesicular glutamate release from central axons contributes to myelin damage. Nat Commun 9, 1032, doi:10.1038/s41467-018-03427-1 (2018). [PubMed: 29531223]
6. Ge WP, Yang XJ, Zhang Z, Wang HK, Shen W, Deng QD et al. Long-term potentiation of neuron-glia synapses mediated by Ca2+-permeable AMPA receptors. Science 312, 1533–1537, doi:10.1126/science.1124669 (2006). [PubMed: 16763153]
7. Sakry D, Yigit H, Dimou L & Trotter J Oligodendrocyte precursor cells synthesize neuromodulatory factors. PloS one 10, e0127222, doi:10.1371/journal.pone.0127222 (2015). [PubMed: 25966014]
8. Birey F, Kloc M, Chavali M, Hussein I, Wilson M, Christoffel DJ et al. Genetic and Stress-Induced Loss of NG2 Glia Triggers Emergence of Depressive-like Behaviors through Reduced Secretion of FGF2. Neuron 88, 941–956, doi:10.1016/j.neuron.2015.10.046 (2015). [PubMed: 26606998]
9. Nagy C, Maitra M, Tanti A, Suderman M, Théroux JF, Davoli MA et al. Single-nucleus transcriptomics of the prefrontal cortex in major depressive disorder implicates oligodendrocyte precursor cells and excitatory neurons. Nature neuroscience 23, 771–781, doi:10.1038/s41593-020-0621-y (2020). [PubMed: 32341540]
10. Liu J, Dietz K, DeLoyht JM, Pedre X, Kelkar D, Kaur J et al. Impaired adult myelination in the prefrontal cortex of socially isolated mice. Nature neuroscience 15, 1621–1623, doi:10.1038/nn.3263 (2012). [PubMed: 23143512]
11. Makinodan M, Ikawa D, Yamamuro K, Yamashita Y, Toritsuka M, Kimoto S et al. Effects of the mode of re-socialization after juvenile social isolation on medial prefrontal cortex myelination and function. Sci Rep 7, 5481, doi:10.1038/s41598-017-05632-2 (2017). [PubMed: 28710465]
12. Zhang H, Yan G, Xu H, Fang Z, Zhang J, Zhang J et al. The recovery trajectory of adolescent social defeat stress-induced behavioral, (1)H-MRS metabolites and myelin changes in Balb/c mice. Sci Rep 6, 27906, doi:10.1038/srep27906 (2016). [PubMed: 27283029]
13. Yang Y, Zhang Y, Luo F & Li B Chronic stress regulates $NG2^+$ cell maturation and myelination in the prefrontal cortex through induction of death receptor 6. Exp Neurol 277, 202–214, doi:10.1016/j.expneurol.2016.01.003 (2016). [PubMed: 26772637]

14. Lehmann ML, Weigel TK, Elkahloun AG & Herkenham M Chronic social defeat reduces myelination in the mouse medial prefrontal cortex. Sci Rep 7, 46548, doi:10.1038/srep46548 (2017). [PubMed: 28418035]
15. Bonnefil V, Dietz K, Amatruda M, Wentling M, Aubry AV, Dupree JL et al. Region-specific myelin differences define behavioral consequences of chronic social defeat stress in mice. Elife 8, e40855, doi:10.7554/eLife.40855 (2019). [PubMed: 31407664]
16. Bae JN, MacFall JR, Krishnan KR, Payne ME, Steffens DC & Taylor WD Dorsolateral prefrontal cortex and anterior cingulate cortex white matter alterations in late-life depression. Biol Psychiatry 60, 1356–1363, doi:10.1016/j.biopsych.2006.03.052 (2006). [PubMed: 16876144]
17. Aston C, Jiang L & Sokolov BP Transcriptional profiling reveals evidence for signaling and oligodendroglial abnormalities in the temporal cortex from patients with major depressive disorder. Mol Psychiatry 10, 309–322, doi:10.1038/sj.mp.4001565 (2005). [PubMed: 15303102]
18. van Velzen LS, Kelly S, Isaev D, Aleman A, Aftanas LI, Bauer J et al. White matter disturbances in major depressive disorder: a coordinated analysis across 20 international cohorts in the ENIGMA MDD working group. Mol Psychiatry 25, 1511–1525, doi:10.1038/s41380-019-0477-2 (2020). [PubMed: 31471575]
19. Euston DR, Gruber AJ & McNaughton BL The role of medial prefrontal cortex in memory and decision making. Neuron 76, 1057–1070, doi:10.1016/j.neuron.2012.12.002 (2012). [PubMed: 23259943]
20. Russo SJ & Nestler EJ The brain reward circuitry in mood disorders. Nat Rev Neurosci 14, 609–625, doi:10.1038/nrn3381 (2013). [PubMed: 23942470]
21. Dias-Ferreira E, Sousa JC, Melo I, Morgado P, Mesquita AR, Cerqueira JJ et al. Chronic stress causes frontostriatal reorganization and affects decision-making. Science 325, 621–625, doi:10.1126/science.1171203 (2009). [PubMed: 19644122]
22. Arnsten AF Stress signalling pathways that impair prefrontal cortex structure and function. Nat Rev Neurosci 10, 410–422, doi:10.1038/nrn2648 (2009). [PubMed: 19455173]
23. Elsayed M & Magistretti PJ A New Outlook on Mental Illnesses: Glial Involvement Beyond the Glue. Frontiers in cellular neuroscience 9, 468, doi:10.3389/fncel.2015.00468 (2015). [PubMed: 26733803]
24. Golden SA, Covington HE, Berton O & Russo SJ A standardized protocol for repeated social defeat stress in mice. Nature Protocols 6, 1183–1191, doi:10.1038/nprot.2011.361 (2011). [PubMed: 21799487]
25. Madisen L, Zwingman TA, Sunkin SM, Oh SW, Zariwala HA, Gu H et al. A robust and high-throughput Cre reporting and characterization system for the whole mouse brain. Nature neuroscience 13, 133–140, doi:10.1038/nn.2467 (2010). [PubMed: 20023653]
26. Riva-Posse P, Choi KS, Holtzheimer PE, McIntyre CC, Gross RE, Chaturvedi A et al. Defining Critical White Matter Pathways Mediating Successful Subcallosal Cingulate Deep Brain Stimulation for Treatment-Resistant Depression. Biological Psychiatry 76, 963–969, doi:10.1016/j.biopsych.2014.03.029 (2014). [PubMed: 24832866]
27. Versace A, Thompson WK, Zhou D, Almeida JR, Hassel S, Klein CR et al. Abnormal left and right amygdala-orbitofrontal cortical functional connectivity to emotional faces: state versus trait vulnerability markers of depression in bipolar disorder. Biological psychiatry 67, 422–431 (2010). [PubMed: 20159144]
28. Keirstead HS, Levine JM & Blakemore WF Response of the oligodendrocyte progenitor cell population (defined by NG2 labelling) to demyelination of the adult spinal cord. Glia 22, 161–170 (1998). [PubMed: 9537836]
29. Wang J & Tsirka SE Neuroprotection by inhibition of matrix metalloproteinases in a mouse model of intracerebral haemorrhage. Brain 128, 1622–1633, doi:10.1093/brain/awh489 (2005). [PubMed: 15800021]
30. Lehmann ML, Weigel TK, Poffenberger CN & Herkenham M The Behavioral Sequelae of Social Defeat Require Microglia and Are Driven by Oxidative Stress in Mice. The Journal of neuroscience : the official journal of the Society for Neuroscience 39, 5594–5605, doi:10.1523/jneurosci.0184-19.2019 (2019). [PubMed: 31085604]

31. Butts BD, Houde C & Mehmet H Maturation-dependent sensitivity of oligodendrocyte lineage cells to apoptosis: implications for normal development and disease. Cell Death & Differentiation 15, 1178–1186, doi:10.1038/cdd.2008.70 (2008). [PubMed: 18483490]
32. Spaas J, van Veggel L, Schepers M, Tiane A, van Horssen J, Wilson DM et al. Oxidative stress and impaired oligodendrocyte precursor cell differentiation in neurological disorders. Cellular and Molecular Life Sciences 78, 4615–4637, doi:10.1007/s00018-021-03802-0 (2021). [PubMed: 33751149]
33. Way SW, Podojil JR, Clayton BL, Zaremba A, Collins TL, Kunjamma RB et al. Pharmaceutical integrated stress response enhancement protects oligodendrocytes and provides a potential multiple sclerosis therapeutic. Nature Communications 6, 6532, doi:10.1038/ncomms7532 (2015).
34. Ron D & Walter P Signal integration in the endoplasmic reticulum unfolded protein response. Nature reviews Molecular cell biology 8, 519–529 (2007). [PubMed: 17565364]
35. Schmaal L, Pozzi E, T CH, van Velzen LS, Veer IM, Opel N et al. ENIGMA MDD: seven years of global neuroimaging studies of major depression through worldwide data sharing. Transl Psychiatry 10, 172, doi:10.1038/s41398-020-0842-6 (2020). [PubMed: 32472038]
36. Jäkel S, Agirre E, Mendanha Falcão A, van Bruggen D, Lee KW, Knuesel I et al. Altered human oligodendrocyte heterogeneity in multiple sclerosis. Nature 566, 543–547, doi:10.1038/s41586-019-0903-2 (2019). [PubMed: 30747918]
37. Trapnell C, Cacchiarelli D, Grimsby J, Pokharel P, Li S, Morse M et al. The dynamics and regulators of cell fate decisions are revealed by pseudotemporal ordering of single cells. Nat Biotechnol 32, 381–386, doi:10.1038/nbt.2859 (2014). [PubMed: 24658644]
38. Li Q & Barres BA Microglia and macrophages in brain homeostasis and disease. Nature Reviews Immunology 18, 225 (2018).
39. van der Poel M, Ulas T, Mizee MR, Hsiao C-C, Miedema SSM, Adeliaet al. Transcriptional profiling of human microglia reveals grey–white matter heterogeneity and multiple sclerosis-associated changes. Nature Communications 10, 1139, doi:10.1038/s41467-019-08976-7 (2019).
40. Schetters STT, Gomez-Nicola D, Garcia-Vallejo JJ & Van Kooyk Y Neuroinflammation: Microglia and T Cells Get Ready to Tango. Frontiers in Immunology 8, doi:10.3389/fimmu.2017.01905 (2018). [PubMed: 29403492]
41. Harrington EP, Bergles DE & Calabresi PA Immune cell modulation of oligodendrocyte lineage cells. Neurosci Lett 715, 134601–134601, doi:10.1016/j.neulet.2019.134601 (2020). [PubMed: 31693930]
42. Ridler C Oligodendrocytes — active accomplices in MS pathogenesis? Nature Reviews Neurology 15, 3–3, doi:10.1038/s41582-018-0111-y (2019). [PubMed: 30531818]
43. Krishnan V & Nestler EJ Animal models of depression: molecular perspectives. Curr topics behav neurosciences 7, 121–147, doi:10.1007/7854_2010_108 (2011).
44. Banasr M, Valentine GW, Li XY, Gourley SL, Taylor JR & Duman RS Chronic unpredictable stress decreases cell proliferation in the cerebral cortex of the adult rat. Biol Psychiatry 62, 496–504, doi:10.1016/j.biopsych.2007.02.006 (2007). [PubMed: 17585885]
45. Hill RA & Nishiyama A NG2 cells (polydendrocytes): listeners to the neural network with diverse properties. Glia 62, 1195–1210, doi:10.1002/glia.22664 (2014). [PubMed: 24753030]
46. Nishiyama A, Komitova M, Suzuki R & Zhu X Polydendrocytes (NG2 cells): multifunctional cells with lineage plasticity. Nature Reviews Neuroscience 10, 9–22, doi:10.1038/nrn2495 (2009). [PubMed: 19096367]
47. Nie X, Kitaoka S, Tanaka K, Segi-Nishida E, Imoto Y, Ogawa A et al. The Innate Immune Receptors TLR2/4 Mediate Repeated Social Defeat Stress-Induced Social Avoidance through Prefrontal Microglial Activation. Neuron 99, 464–479.e467, doi:10.1016/j.neuron.2018.06.035 (2018). [PubMed: 30033154]
48. Kokkosis AG & Tsirka SE Neuroimmune mechanisms and sex/gender-dependent effects in the pathophysiology of mental disorders. Journal of Pharmacology and Experimental Therapeutics 375, 175–192 (2020). [PubMed: 32661057]
49. Miller AH & Raison CL The role of inflammation in depression: from evolutionary imperative to modern treatment target. Nat Rev Immunol 16, 22–34, doi:10.1038/nri.2015.5 (2016). [PubMed: 26711676]

50. Mecha M, Torrao AS, Mestre L, Carrillo-Salinas FJ, Mechoulam R & Guaza C Cannabidiol protects oligodendrocyte progenitor cells from inflammation-induced apoptosis by attenuating endoplasmic reticulum stress. Cell Death & Disease 3, e331–e331, doi:10.1038/cddis.2012.71 (2012). [PubMed: 22739983]
51. Harding HP, Zhang Y, Zeng H, Novoa I, Lu PD, Calfon M et al. An Integrated Stress Response Regulates Amino Acid Metabolism and Resistance to Oxidative Stress. Molecular Cell 11, 619–633, doi:10.1016/S1097-2765(03)00105-9 (2003). [PubMed: 12667446]
52. Way SW & Popko B Harnessing the integrated stress response for the treatment of multiple sclerosis. The Lancet Neurology 15, 434–443, doi:10.1016/S1474-4422(15)00381-6 (2016). [PubMed: 26873788]
53. Costa-Mattioli M & Walter P The integrated stress response: From mechanism to disease. Science 368, doi:10.1126/science.aat5314 (2020).
54. Han J, Back SH, Hur J, Lin YH, Gildersleeve R, Shan J et al. ER-stress-induced transcriptional regulation increases protein synthesis leading to cell death. Nat Cell Biol 15, 481–490, doi:10.1038/ncb2738 (2013). [PubMed: 23624402]
55. Falcao AM, van Bruggen D, Marques S, Meijer M, Jakel S, Agirre E et al. Disease-specific oligodendrocyte lineage cells arise in multiple sclerosis. Nat Med 24, 1837–1844, doi:10.1038/s41591-018-0236-y (2018). [PubMed: 30420755]
56. Taylor S, Mehina E, White E, Reeson P, Yongblah K, Doyle KP et al. Suppressing Interferon-gamma Stimulates Microglial Responses and Repair of Microbleeds in the Diabetic Brain. The Journal of neuroscience : the official journal of the Society for Neuroscience 38, 8707–8722, doi:10.1523/JNEUROSCI.0734-18.2018 (2018). [PubMed: 30201775]
57. Kirby L, Jin J, Cardona JG, Smith MD, Martin KA, Wang J et al. Oligodendrocyte precursor cells present antigen and are cytotoxic targets in inflammatory demyelination. Nature Communications 10, 3887, doi:10.1038/s41467-019-11638-3 (2019).
58. Rivers LE, Young KM, Rizzi M, Jamen F, Psachoulia K, Wade A et al. PDGFRA/NG2 glia generate myelinating oligodendrocytes and piriform projection neurons in adult mice. Nature neuroscience 11, 1392–1401, doi:10.1038/nn.2220 (2008). [PubMed: 18849983]
59. Krishnan V, Han MH, Graham DL, Berton O, Renthal W, Russo SJ et al. Molecular adaptations underlying susceptibility and resistance to social defeat in brain reward regions. Cell 131, 391–404, doi:10.1016/j.cell.2007.09.018 (2007). [PubMed: 17956738]
60. Ferlemi AV, Avgoustatos D, Kokkosis AG, Protonotarios V, Constantinou C & Margarity M Lead-induced effects on learning/memory and fear/anxiety are correlated with disturbances in specific cholinesterase isoform activity and redox imbalance in adult brain. Physiol Behav 131, 115–122, doi:10.1016/j.physbeh.2014.04.033 (2014). [PubMed: 24768645]
61. Kokkosis A, Valais K, Mullahy M & Tsirka SE Depression Mediated By Inflammatory Responses To Chronic Stress. The FASEB Journal 34, 1–1 (2020).
62. Castagne V, Moser P, Roux S & Porsolt RD Rodent models of depression: forced swim and tail suspension behavioral despair tests in rats and mice. Curr Protoc Pharmacol Chapter 5, Unit 5 8, doi:10.1002/0471141755.ph0508s49 (2010).
63. Castagne V, Moser P, Roux S & Porsolt RD Rodent models of depression: forced swim and tail suspension behavioral despair tests in rats and mice. Curr Protoc Neurosci Chapter 8, Unit 8 10A, doi:10.1002/0471142301.ns0810as55 (2011).
64. Goshen I, Kreisel T, Ben-Menachem-Zidon O, Licht T, Weidenfeld J, Ben-Hur T et al. Brain interleukin-1 mediates chronic stress-induced depression in mice via adrenocortical activation and hippocampal neurogenesis suppression. Molecular Psychiatry 13, 717–728, doi:10.1038/sj.mp.4002055 (2008). [PubMed: 17700577]
65. Zanos P, Moaddel R, Morris PJ, Georgiou P, Fischell J, Elmer GI et al. NMDAR inhibition-independent antidepressant actions of ketamine metabolites. Nature 533, 481–486, doi:10.1038/nature17998 (2016). [PubMed: 27144355]
66. Camargo A, Pazini FL, Rosa JM, Wolin IA, Moretti M, Rosa PB et al. Augmentation effect of ketamine by guanosine in the novelty-suppressed feeding test is dependent on mTOR signaling pathway. Journal of psychiatric research 115, 103–112 (2019). [PubMed: 31128500]

67. Zeng C, Pan F, Jones LA, Lim MM, Griffin EA, Sheline YI et al. Evaluation of 5-ethynyl-2'-deoxyuridine staining as a sensitive and reliable method for studying cell proliferation in the adult nervous system. Brain Res 1319, 21–32, doi:10.1016/j.brainres.2009.12.092 (2010). [PubMed: 20064490]
68. Bindokas VP, Jordán J, Lee CC & Miller RJ Superoxide production in rat hippocampal neurons: selective imaging with hydroethidine. The Journal of neuroscience : the official journal of the Society for Neuroscience 16, 1324–1336, doi:10.1523/jneurosci.16-04-01324.1996 (1996). [PubMed: 8778284]
69. Nazarewicz RR, Bikineyeva A & Dikalov SI Rapid and specific measurements of superoxide using fluorescence spectroscopy. J Biomol Screen 18, 498–503, doi:10.1177/1087057112468765 (2013). [PubMed: 23190737]
70. Schindelin J, Arganda-Carreras I, Frise E, Kaynig V, Longair M, Pietzsch T et al. Fiji: an open-source platform for biological-image analysis. Nature Methods 9, 676–682, doi:10.1038/nmeth.2019 (2012). [PubMed: 22743772]
71. Chavali M, Klingener M, Kokkosis AG, Garkun Y, Felong S, Maffei A et al. Non-canonical Wnt signaling regulates neural stem cell quiescence during homeostasis and after demyelination. Nat Commun 9, 36, doi:10.1038/s41467-017-02440-0 (2018). [PubMed: 29296000]
72. Eyermann C, Czaplinski K & Colognato H Dystroglycan promotes filopodial formation and process branching in differentiating oligodendroglia. J Neurochem 120, 928–947, doi:10.1111/j.1471-4159.2011.07600.x (2012). [PubMed: 22117643]
73. Butler A, Hoffman P, Smibert P, Papalexi E & Satija R Integrating single-cell transcriptomic data across different conditions, technologies, and species. Nat Biotechnol 36, 411–420, doi:10.1038/nbt.4096 (2018). [PubMed: 29608179]
74. Stuart T, Butler A, Hoffman P, Hafemeister C, Papalexi E, Mauck WM 3rd et al. Comprehensive Integration of Single-Cell Data. Cell 177, 1888–1902 e1821, doi:10.1016/j.cell.2019.05.031 (2019). [PubMed: 31178118]
75. Kolde R Pheatmap: Pretty Heatmaps. R Package version 1.0.12. https://CRAN.R-project.org/package=pheatmap (2019).
76. Qiu X, Hill A, Packer J, Lin D, Ma YA & Trapnell C Single-cell mRNA quantification and differential analysis with Census. Nat Methods 14, 309–315, doi:10.1038/nmeth.4150 (2017). [PubMed: 28114287]
77. Yu G, Wang L-G, Han Y & He Q-Y clusterProfiler: an R package for comparing biological themes among gene clusters. Omics: a journal of integrative biology 16, 284–287 (2012). [PubMed: 22455463]
78. Shapiro SS & Wilk MB An analysis of variance test for normality (complete samples). Biometrika 52, 591–611 (1965).
79. The SAGE Dictionary of Statistics. The SAGE Dictionary of Statistics. SAGE Publications, Ltd. (SAGE Publications, Ltd).
80. Doane DP & Seward LE Measuring Skewness: A Forgotten Statistic? J Stat Edu 19, 1–18 (2011).

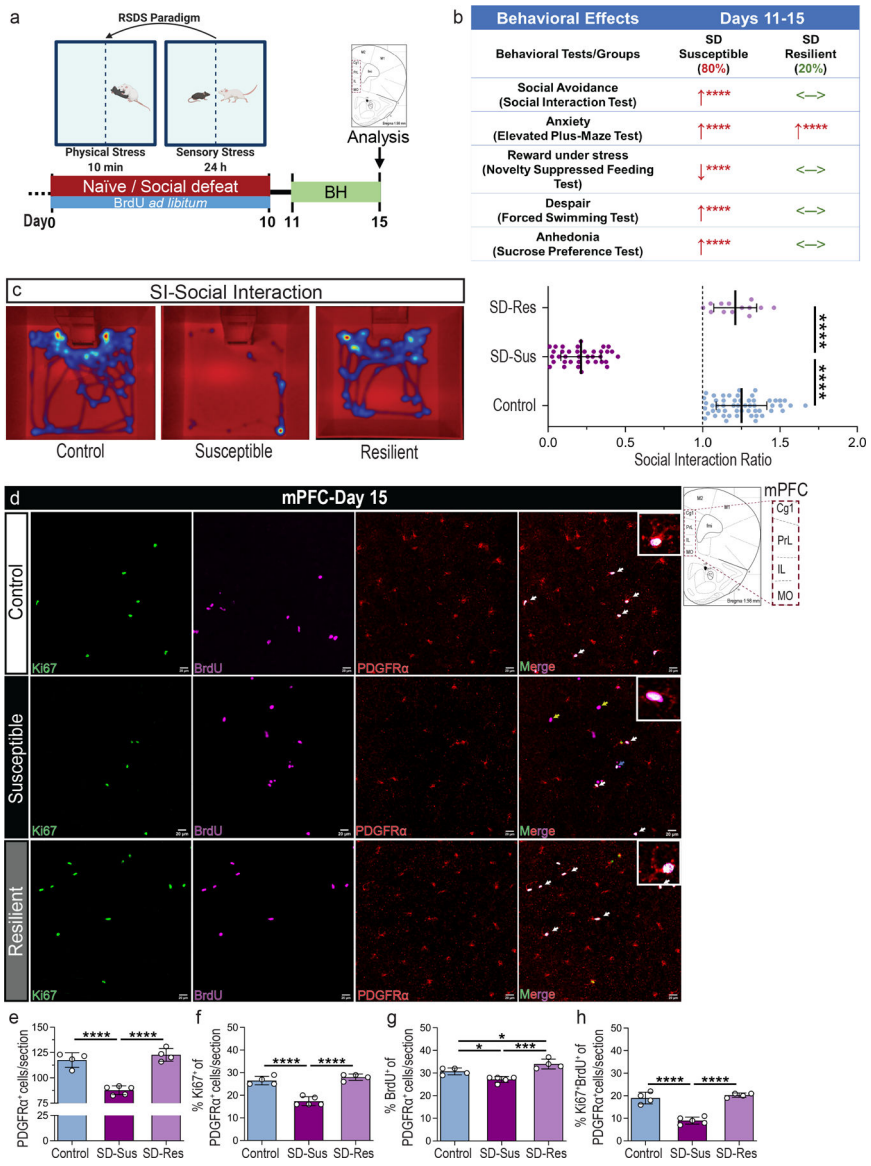

Fig. 1 |. Chronic psychosocial stress induces depressive-like behavior leading to OPC reductions and impaired proliferation in the mPFC.

(**a**) Experimental outline for the repeated social defeat stress (RSDS) paradigm in mice. 5-Bromo-2′-deoxyuridine (BrdU) was administered *ad libitum* throughout the 10 days of RSDS to label proliferating cell populations. Behavioral testing (BH) was performed between D11-D15. (**b**) Summary table with the behavioral effects of chronic stress in Susceptible (SD-Sus) and Resilient (SD-Res) groups. Relative comparisons to the Con groups: ↑ depicts increase, ↓ depicts decrease, <—> depicts no change. (**c**) Representative heatmaps of social interaction (SI) test (left), and SI ratios (right; $F_{2,101} = 565.8$, ****$P \leq 0.0001$). One-way ANOVA with Tukey's multiple comparisons; Con: n=50, SD-Sus: n=37, SD-Res: n=13. (**h**) Representative images of BrdU$^+$ (magenta) label retaining OPCs (PDGFRα$^+$; red) and their current proliferation capacity (Ki67$^+$; green) in mPFC; Scale bars: 20 μm; On the right of (**h**): schematic of the sampled area within the mPFC; red-dashed rectangle line demarcates the regions examined (Cg1, PrL, IL, MO). (**i**) OPC density

(PDGFRα$^+$; $F_{2,10}$ = 46.97, ****$P \leq 0.0001$). (**j**) Percentage of OPC proliferation capacity (PDGFRα$^+$Ki67$^+$) in the total OPC population (% Ki67$^+$ of PDGFRα$^+$; $F_{2,10}$ = 47.05, ****$P \leq 0.0001$) at D15 (**k**) Percentage of OPC proliferation (PDGFRα$^+$BrdU$^+$) during the RSDS (% BrdU$^+$ of PDGFRα$^+$; $F_{2,10}$ = 18.79, ***$P = 0.0004$). (**l**) Percentage of OPC label-retaining cells (PDGFRα$^+$BrdU$^+$Ki67$^+$) proliferating at D15 (% Ki67$^+$BrdU$^+$ of PDGFRα$^+$; $F_{2,10}$ = 53.51, ****$P \leq 0.0001$; indicated by white arrows and displayed in the insets). Yellow arrows in (**h**) depict PDGFRα$^-$BrdU$^+$ retaining cells (possibly differentiating OPCs) and blue arrow depicts BrdU retaining cells proliferating at D15 (PDGFRα$^-$BrdU$^+$Ki67$^+$). For panels (**i-l**): one-way ANOVA with Tukey's multiple comparisons; Con: n=4, SD-Sus: n=5, SD-Res: n=4. Data are reported as mean ± S.D; *$P \leq 0.05$, ***$P \leq 0.001$, ****$P \leq$ 0.0001. Statistical analysis details are reported in Supplementary Table 1; mPFC: medial prefrontal cortex; Cg1: cingulate cortex; PrL: prelimbic cortex; IL: Infralimbic cortex; MO: medial orbital cortex; M1, M2: motor cortices.

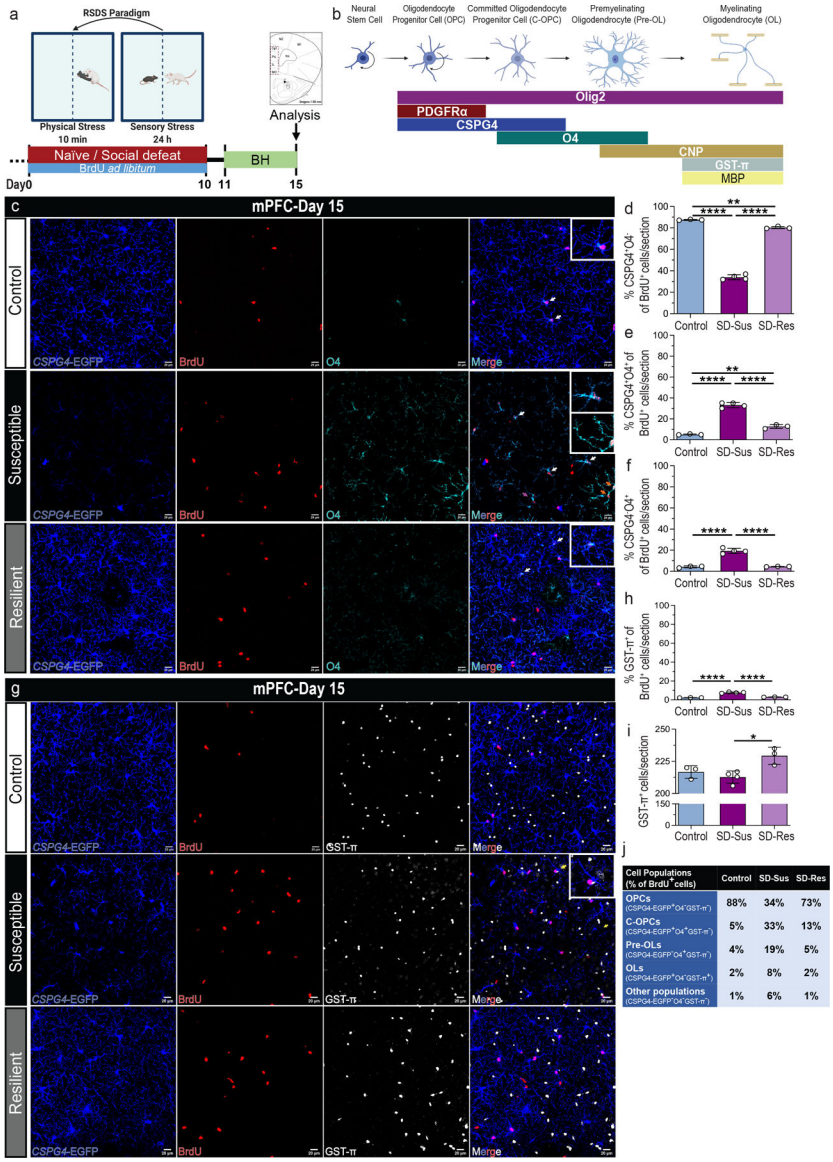

Fig. 2 |. Chronic psychosocial stress induces the maturation of label-retaining OPCs into OLs post-RSDS in the mPFC.

(**a**) Experimental outline of RSDS and BrdU administration. (**b**) Graphical representation of oligodendroglial lineage (OLN) stage and respective markers used in this study [Oligodendrocyte progenitor cells (OPCs), committed oligodendrocyte progenitor cells (C-OPCs), premyelinating immature oligodendrocytes (Pre-OLs) and myelinating mature oligodendrocytes (OLs)]. (**c**) Representative images of $BrdU^+$ (red) label-retaining OPCs ($CSPG4^+$; blue) and C-OPCs/Pre-OLs ($O4^+$; cyanine) in mPFC; Scale bars: 100 μm (left), 20 μm (right). (**d**) Percentage of BrdU-retaining OPCs ($BrdU^+CSPG4^+O4^-$) in the total $BrdU^+$ population (% $CSPG4^+O4^-$ of $BrdU^+$; $F_{2,7} = 1146$, $^{****}P \leq 0.0001$). (**e**) Percentage of BrdU-retaining C-OPCs ($BrdU^+CSPG4^+O4^+$) in the total $BrdU^+$ population [% $CSPG4^+O4^+$ of $BrdU^+$; $F_{2,7} = 196.9$, $^{****}P \leq 0.0001$; indicated by white arrows and displayed in the top insets of (**c**)]. (**f**) Percentage of BrdU-retaining Pre-OLs ($BrdU^+CSPG4^-O4^+$) in the total $BrdU^+$ population [% $CSPG4^-O4^+$ of $BrdU^+$; $F_{2,7} = 102.7$,

*****P* ≤ 0.0001; indicated by red arrows and displayed in the bottom inset of SD-Sus group in (**c**)]. (**g**) Representative images of $BrdU^+$ (red) retaining OPCs ($CSPG4^+$; blue) and OLs (GST-π^+; grey) in mPFC; Scale bars: 100 μm (left), 20 μm (right). (**h**) Percentage of BrdU-retaining OLs ($BrdU^+$GST-π^+) in the total $BrdU^+$ population [% GST-π^+ of $BrdU^+$; $F_{2,7}$ = 166.9, *****P* ≤ 0.0001; indicated by yellow arrows and displayed in the top inset of SD-Sus group in (**g**)]. (**i**) OL density (GST-π^+; $F_{2,7}$ = 8.37, **P* = 0.0139 (**j**) Summary table with percentages of each OLN cell population versus the total number of $BrdU^+$ cells. IHC: Con: *n*=4, SD-Sus: *n*=5, SD-Res: *n*=4; Scale bars: 100 μm (left), 20 μm (right). For panels (**d-f, h-I**): one-way ANOVA with Tukey's multiple comparisons; Con: *n*=3, SD-Sus: *n*=4, SD-Res: *n*=3. Data are reported as mean ± S.D; **P* ≤ 0.05, ***P* ≤ 0.01, *****P* ≤ 0.0001. Statistical analysis details are reported in Supplementary Table 1.

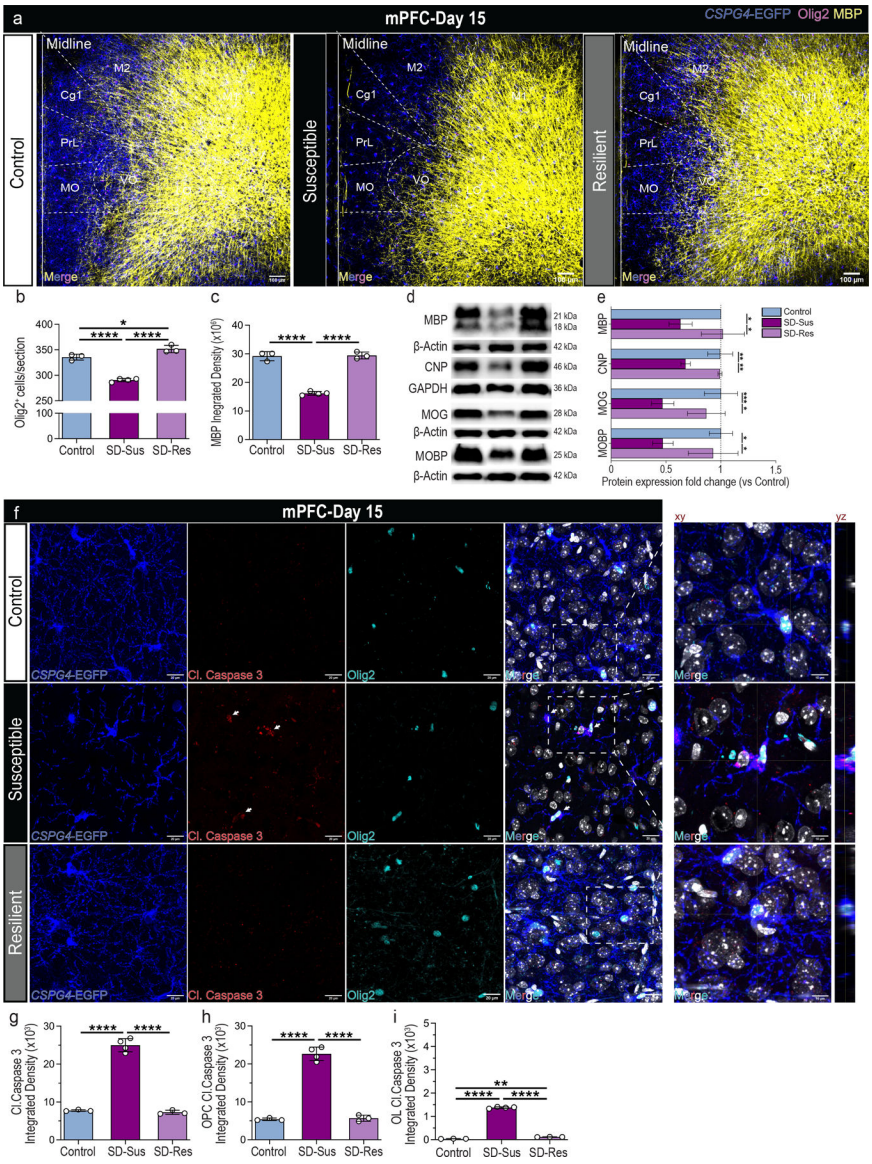

Fig. 3 |. Myelin deficits and oligodendroglial apoptosis are induced in response to chronic psychosocial stress.

(**a**) Representative images of OPCs (CSPG4$^+$; blue), pan-OLN marker (Olig2$^+$; magenta) and MBP$^+$ (yellow) myelin marker in mPFC; Overlayed mouse brain areas examined at Bregma: 2.10 μm; Scale bar: 100 μm. (**b**) Pan-OLN cell density (Olig2$^+$; $F_{2,7}$ = 120.7, $^{****}P \leq 0.0001$). (**c**) Myelin integrated density (MBP$^+$; $F_{2,7}$ = 159.2, $^{****}P \leq 0.0001$). (**d**) Immunoblot analyses of mPFC assessing the protein levels for the myelin markers MBP, CNP, MOG and MOBP at D15 post RSDS. (**e**) MBP ($F_{2,6}$ = 8.8583, $^{*}P$ = 0.0174), CNP ($F_{2,6}$ = 20.64, $^{**}P$ = 0.002), MOG ($F_{2,9}$ = 16.12, $^{**}P$ = 0.0011), MOBP ($F_{2,5}$ = 13.05, $^{*}P$ = 0.0104). For panels (**b, c, e**): one-way ANOVA with Tukey's multiple comparisons; For panels (**b, c**): Con: n=4, SD-Sus: n=5, SD-Res: n=4; For panel (**e**): Con: n=3–5, SD-Sus: n=3–4, SD-Res: n=2–3. (**f**) Representative images of microglia OPCs (CSPG4-EGFP$^+$; blue), cell apoptosis (Cleaved Caspase-3$^+$; red), pan-OLN marker (Olig2$^+$; cyanine) and DAPI staining (nuclei; grey) in mPFC; Scale bars: 20 μm (left), 10 μm (xy representative

planes on the right); yz planes depict OPC with Cl. Caspase-3 expression. (**g**) Total Cl. Caspase-3 integrated density ($F_{2,7}$ = 261.20, ****$P \leq 0.0001$). (h) OPC-specific Cl. Caspase-3 integrated density (CSPG4^{+}Olig2^{+}Cl.Caspase3^{+}; $F_{2,7}$ = 221.80, ****$P \leq 0.0001$). (i) OL-specific Cl. Caspase-3 integrated density (CSPG4^{-}Olig2^{+}Cl.Caspase3^{+}; $F_{2,7}$ = 4226, ****$P \leq 0.0001$). For panels (**g-i**): one-way ANOVA with Tukey's multiple comparisons; Con: n=3, SD-Sus: n=4, SD-Res: n=3. Data are reported as mean ± S.D; *$P \leq 0.05$, **$P \leq 0.01$, ***$P \leq 0.001$, ****$P \leq 0.0001$. Statistical analysis details are reported in Supplementary Table 1; DHE: Dihydroethidium. The representative gels displayed in panels (d) are cropped the original images are shown in Supplementary Fig. 18. Statistical analysis details are reported in Supplementary Table 1.

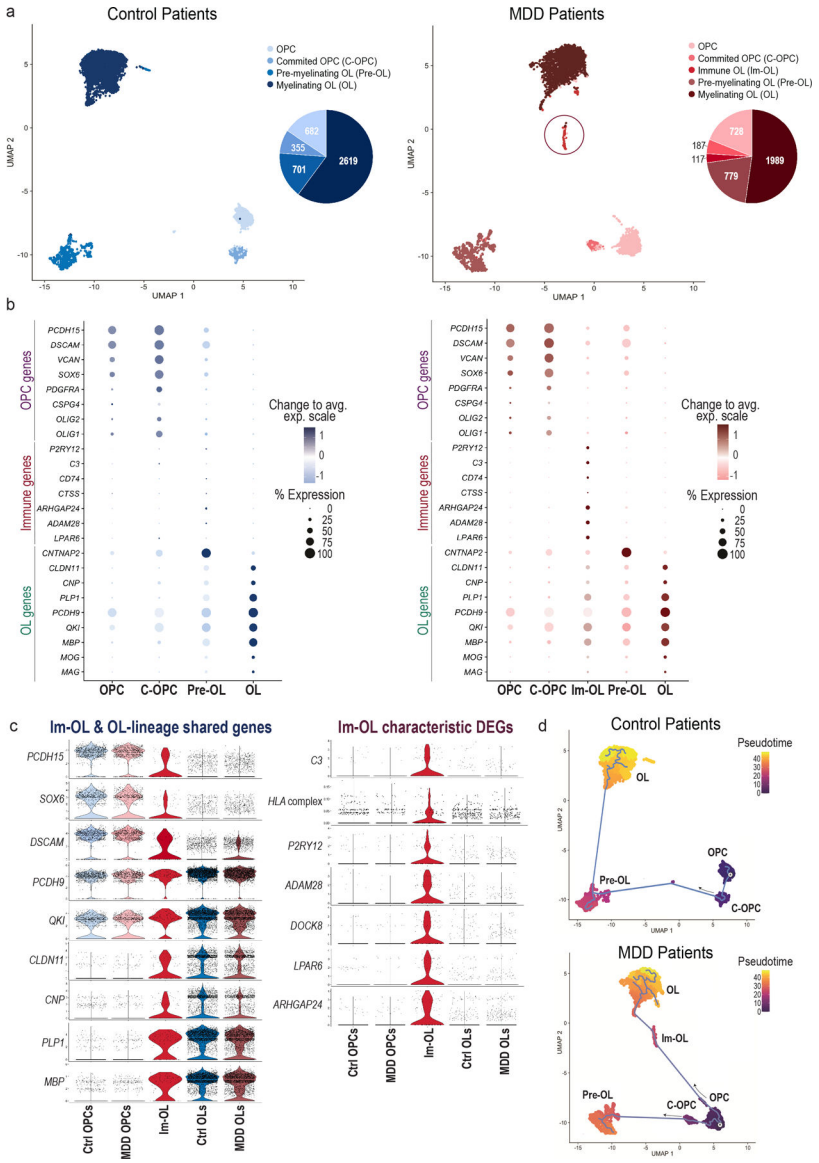

Fig. 4 |. Single-nucleus transcriptomic characterization of oligodendroglial-lineage populations in the dlPFC of MDD and Control patients.

(**a**) Uniform Manifold Approximation and Projection (UMAP) clustering of oligodendroglial lineage (OLN) cells per condition: Control (blue shades) and MDD (red shades) patients (n.neighbors = 20, min.dist = 0.2). OLN clusters were annotated and subsetted based on well-established marker genes (see Methods) for each condition: four common clusters (OPCs, C-OPCs, Pre-OLs, OLs) and an MDD-specific cluster (Im-OL in red circle) were identified from the analysis. On the right of each UMAP clustering, pie charts indicate the raw cell numbers from each cluster. (**b**) Dotplots depicting the top expressed known marker genes [early OLN genes (OPC genes), immune-related genes (Immune genes) and late OLN genes (OL genes)] in the clusters of interest. OLN gene markers are color-coded with blue shades in control and with red shades in MDD patients. The color intensity represents the average expression levels (Change to avg. exp. scale), while the size of the dots represents the percentage of cells within each cluster expressing the gene (%

Expression). (**c**) Violin plot of top expressed oligodendroglial-lineage marker genes shared in Im-OL and OLN clusters and divided per condition [Control (blue) and MDD (red)]. (**d**) Violin plot of characteristic differentially expressed genes (DEGs) in Im-OL, divided per condition (Control and MDD). The HLA complex includes grouped gene scoring from the human leukocyte antigen (HLA) family; For the violin plots (**c, d**) the OPCs and Committed OPCs clusters are grouped and termed as OPCs. Immature Pre-myelinating OLs and Mature-Myelinating OLs clusters are grouped and termed as OLs; The values extend from minimum to maximum and the *n* value per cluster corresponds to the total no. of cells (represented by dots) for each condition. (**e**) Pseudotime trajectory analysis of oligodendroglial developmental stages divided per condition [Control (top), MDD (bottom)]. "R" marks the OPCs, the root starting point used for graph learning. The cell color indicates the pseudotime trajectory (pseudotime). OPCs: Oligodendrocyte progenitor cells; C-OPCs: committed-oligodendrocyte progenitor cells; Pre-OLs: premyelinating immature oligodendrocytes; OLs: myelinating mature oligodendrocytes (OLs); Im-OL: immune-oligodendrocytes; dlPFC: dorsolateral prefrontal cortex.

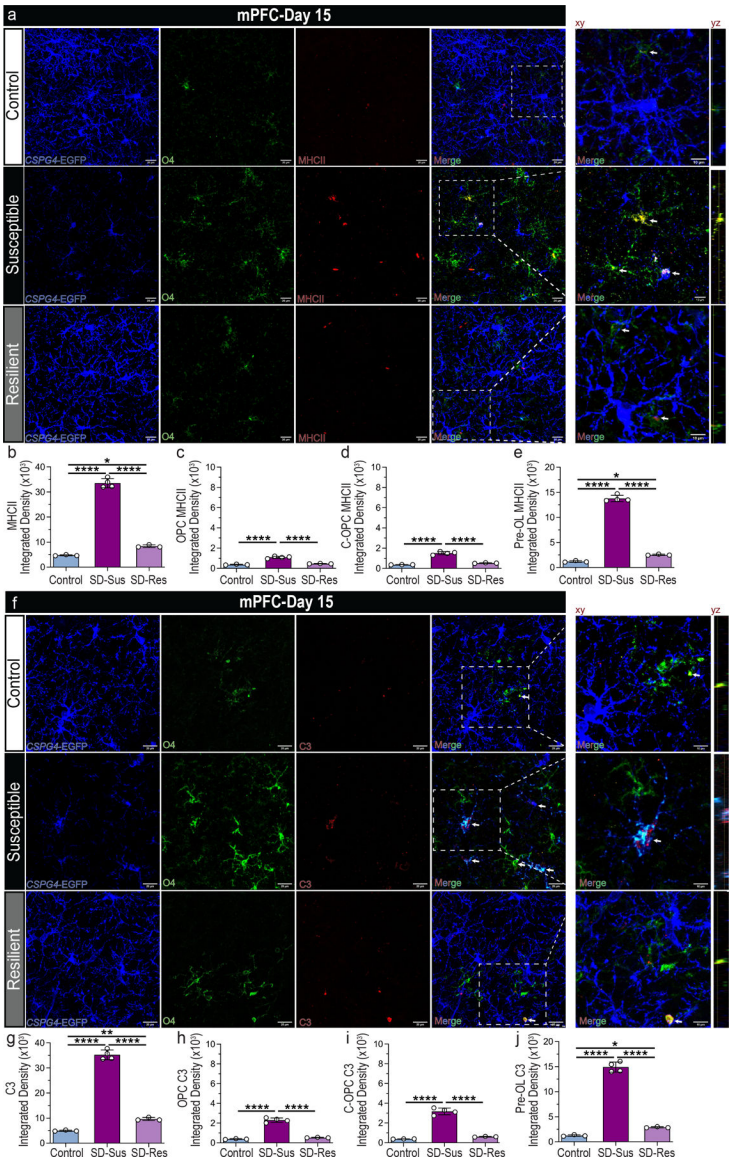

Fig. 5 |. Oligodendroglial expression of MHCII and complement C3 in mPFC post RSDS.

(**a**) Representative images of OPCs (CSPG4$^+$; blue), C-OPCs/Pre-OLs (O4$^+$; green) and MHCII (red; indicated by white arrows) antigen presentation marker in mPFC. Scale bars: 20 μm (left), 10 μm (xy representative planes on the right); yz planes depict oligodendroglia with MHCII expression. (**b-e**) Integrated densities for various markers. (**b**) Total MHCII ($F_{2,7}$ = 572.80, $^{****}P \leq 0.0001$). (**c**) OPC-specific MHCII (CSPG4$^+$O4$^-$MHCII$^+$; $F_{2,7}$ = 104.0, $^{****}P \leq 0.0001$). (d) C-OPC specific MHCII (CSPG4$^+$O4$^+$MHCII$^+$; $F_{2,7}$ = 121.1, $^{****}P \leq 0.0001$). (**e**) Pre-OL-specific MHCII (CSPG4$^-$O4$^+$MHCII$^+$; $F_{2,7}$ = 944.0, $^{****}P \leq 0.0001$). (**f**) Representative images of OPCs (CSPG4$^+$; blue), C-OPCs/Pre-OLs (O4$^+$; green) and complement C3 expression (red; indicated by white arrows) in mPFC. Scale bars: 20 μm (left), 10 μm (xy representative planes on the right); yz planes depict oligodendroglia with complement C3 expression (**g-j**) Integrated densities for various markers. (**g**) Total complement C3 ($F_{2,7}$ = 553.50, $^{****}P \leq 0.0001$). (h) OPC-specific C3 (CSPG4$^+$O4$^-$C3$^+$;

$F_{2,7}$ = 186.3, ****$P \leq 0.0001$). (**i**) C-OPC specific C3 ($CSPG4^{+}O4^{+}C3^{+}$; $F_{2,7}$ = 176.1, ****$P \leq 0.0001$). (j) Pre-OL-specific C3 ($CSPG4^{-}O4^{+}C3^{+}$; $F_{2,7}$ = 454.1, ****$P \leq 0.0001$). For panels (**b-e**, **g-j**): one-way ANOVA with Tukey's multiple comparisons. Con: n=3, SD-Sus: n=4, SD-Res: n=3; Data are reported as mean ± S.D; *$P \leq 0.05$, **$P \leq 0.01$, ****$P \leq 0.0001$. Statistical analysis details are reported in Supplementary Table 1.